MicroRNA166-REVOLUTA-auxin module affects tuber shape, color and productivity in potato

Nikita Sunil Patil[1], Arati Vasav[1], Bhavani Natarajan[1,2], Gourav Arora[1,3], Jyoti Kumari[1] and Anjan K. Banerjee[1*]

[1] Biology Division, Indian Institute of Science Education and Research (IISER) Pune, Dr. Homi Bhabha Road, Maharashtra, India

[2] Department of Plant Sciences, University of Cambridge, Downing Street, Cambridge CB2 3EA, UK

[3]Department of Plant Developmental Biology, Max Planck Institute for Plant Breeding Research, Cologne, Germany

* Corresponding author

Prof. Anjan K. Banerjee

E-mail: akb@iiserpune.ac.in

Tel: +91-20-25908057

The author responsible for distribution of materials integral to the findings presented in this article in accordance with the policy described in the Instructions for Authors (https://academic.oup.com/plphys/pages/General-Instructions) is Prof. Anjan K. Banerjee.

Summary

Tuber shape and size are important traits in potato. Although several factors governing tuberization have been well studied, the molecular mechanisms regulating the tuber shape and size are still elusive. Here, we demonstrate that suppression of *miR166*, which targets class III HD-ZIP transcription factors, alters tuber morphology and productivity in potato. Target mimicry of *miR166* (MIM166) in *Solanum tuberosum* ssp. *Andigena* resulted in elongated, pigmented tubers with reduced yield under short-day conditions. Transcriptome profiling of the tuberizing stolons - swollen head *vs*. stalk revealed differential expression of auxin-, cytokinin-, and gibberellin-associated genes, consistent with altered hormone levels. The coloured tubers from MIM166 line exhibited differential accumulation of cyanidin 3-glucoside, pelargonidin 3-glucoside, and delphinidin 3-glucoside. Tuber productivity in these lines was reduced possibly due to the decreased expression of *SWEET11b* and distorted vascular structures. Further, the *miR166* target- *StREVOLUTA* exhibited dynamic expression during stolon-to-tuber transition, and could modulate *StYUCCA7* expression, an auxin biosynthesis gene. Increased pigmentation and auxin accumulation in MIM166, reduced expression of auxin biosynthesis genes in REVOLUTA antisense, and low tuber yield collectively suggest *miR166*-REV as a regulatory module of auxin homeostasis in differentiating stolons that influences tuber morphology. These results reveal a previously unrecognized miRNA-mediated pathway governing storage organ shape, and extends the functional scope of the *miR166*-HD-ZIP III module beyond organ polarity.

Significance statement

Limited studies describe the molecular mechanisms regulating tuber shape in storage organ development. Here, we show that the *miR166*-REVOLUTA-auxin network has significant regulatory roles in potato development, influencing tuber shape, pigmentation, and productivity. These findings provide insights into molecular control of tuber morphology, uncover hitherto unknown functions of the *miR166*-REVOLUTA module in tuber crops, and broadens our understanding of *miR166*-mediated developmental regulation in plants.

Key words: *miR166*, HD-ZIP III, Potato, Tuber shape, Anthocyanin, auxin, REVOLUTA

Introduction

Potato is one of the most important food crops in the world. The shape and size of potato tuber are key agronomic traits determining the tuber appearance and tuber yield. In plants, organ shape and size is determined by several regulatory genes and hormone signaling networks that affect cell division, cell expansion, and anisotropic growth (Seymour *et al*., 2013; Eldridge *et al*., 2016; Van der Knaap *et al*., 2018; Bu *et al*., 2025). In potato, a belowground modified stem- stolon undergoes developmental transition to form a tuber. Although the genetic and hormonal networks controlling stolon-to-tuber transitions have been extensively studied (Zierer *et al*., 2021), our understanding of the molecular mechanisms determining tuber shape in potato and other storage crops remains limited.

Studies in tomato and rice provided detailed insights into the molecular mechanisms regulating organ shape in fruit and grain development. In tomato, the *OVATE* locus on chromosome 2 controls the transition from round to pear-shaped fruits (Liu *et al*., 2002), while the *SUN*, *SOV1*, and *fs8.1* loci influence fruit elongation through alterations in cell number, and modulation of auxin-related genes (Wang *et al*., 2019). In potato, suppression of an Ovate Family Protein, *StOFP20* (Soltu.DM.09G010420) caused a shift from round to oval tubers. StOFP20 interacts with TONNEAU1 Recruiting Motif proteins, which in turn associate with TON2, potentially affecting cell division and expansion (Ju *et al*., 2023). In rice, grain size is determined by cell number and expansion. Genes such as *GRAIN SIZE 3*, *OsPPKL1*, *OsSPL16*, *GS5*, and the *OsMKK4-OsMPK6* regulate cell proliferation (Fan *et al*., 2006; Mao *et al*., 2010; Hu *et al*., 2012), while *SPL13*, *OsGRF4*, *OsGIF1/2/3*, and *GW7/GL7/SLG7* control cell expansion (Hu *et al*., 2015; Si *et al*., 2016; Che *et al*., 2016; Li *et al*., 2016). In potato, linkage and mapping studies identified significant quantitative trait locus (QTL) for tuber shape on chromosomes 4, 7, and 10 (Park *et al*., 2021). In a study by Fan *et al*. (2022), the *Round* (*Ro*) locus controlling potato tuber shape was fine-mapped on chromosome 10, and five candidate genes potentially responsible for determining round *versus* elongated tuber were identified. In a diploid Andean potato population, candidate genes such as BEL1-like, α-expansin, pectin biosynthesis/modification genes, SCARECROW, and ERF5 were mapped to the QTL on chromosome 10 (Lindqvist-Kreuze *et al*., 2015). Despite multiple studies identifying the QTLs and candidate genes associated with the tuber morphology, their molecular characterization is awaited.

102 Phytohomones, particularly auxin and gibberellin are shown to influence fruit
103 shape in plants. Early work by Stembridge and Morrell (1972) demonstrated that
104 gibberellins (GA_4, GA_7) and cytokinin (6-BAP) increased the length-to-diameter ratio
105 in apples, with combined application being most effective. In tomato, GA_3 application
106 promotes fruit elongation through upregulation of cell elongation genes, whereas
107 inhibition of gibberellin biosynthesis reduces elongation and accelerates ripening
108 (Chen *et al*., 2020). Similarly, the *SUN* locus influences the fruit shape in tomato by
109 modulating auxin biosynthesis, transport, and signaling genes, indicating an interplay
110 between phytohormones and genetic regulators in organ morphology (Wang *et al*.,
111 2019). Thus, organ shape in plants is governed by a coordinated function of the
112 transcriptional regulators, hormone signaling, and cell proliferation/expansion.
113 In potato, the *miR166* family is amongst the most abundantly expressed
114 miRNAs, with a total transcript per million exceeding 600,000, and exhibits tissue-
115 specific and stolon-to-tuber stage-specific expression profiles in potato (Lakhotia *et*
116 *al*., 2014; Kondhare *et al*., 2018). Further analysis of the small RNA sequencing data
117 from Kondhare *et al*. (2018) revealed *miR166* to be differentially accumulated in
118 stolons under long-day (LD; tuber non-inductive) and short-day (SD; tuber inductive)
119 photoperiod. Here, we show that *miR166*-REVOLUTA-auxin module is an important
120 regulator of tuber shape in potato, and modulates key agronomic traits including size,
121 color, and productivity. *miR166* targets *StREVOLUTA*, a HD-ZIP class III
122 transcription factor. StREV binds to the promoter of *StYUCCA7*, an auxin
123 biosynthesis gene and activates its expression. Our work reveals a *miR166*–
124 StREVOLUTA–StYUCCA7 function as one of the key regulatory pathways,
125 providing mechanistic insights into the molecular control of tuber morphology and
126 productivity.
127
128 **Results**
129 **Identification, validation and expression analysis of *miR166* in Potato**
130 Four precursors of *microRNA166* from the miRBase (the microRNA database;
131 http://mirbase.org/) are predicted to form a secondary hairpin loop structure with
132 mature *miR166* in its stem region (MFold; Zuker, 2003) (Figure S1A). To validate the
133 presence of *miR166* precursors (precursors a, b, c and d) in potato, RT-PCR was
134 performed and the amplified products were sequence confirmed (Figure 1A).
135 Precursor-b was the least abundant form, as compared to the other three precursors.

136 Compared to LD, the levels of precursors-a and -c decreased in the stolons under SD
137 photoperiod, while precursor-d increased (Figure 1B-D). The mature forms of all the
138 precursors are identical, except for pre-*miR166*b, wherein it differs by a single base
139 (Figure S1B). In our analysis of small RNA sequencing data from a previous study,
140 we found *miR166* to be the most abundant microRNA in early stolon-to-tuber
141 transition stages and exhibited differential accumulation under short-day (SD; tuber
142 inductive) photoperiod (Kondhare *et al*., 2018) (Figure S2A-B). We detected the 21-
143 bp mature *miR166* by stem-loop endpoint PCR from leaves and stolons of WT potato
144 plants (Figure 1E). The amplified product was verified by sequencing, thus
145 confirming that mature *miR166* is expressed in potato.
146 To determine whether photoperiod affects the accumulation of *miR166*, plants
147 were grown in soil under long-day (LD; tuber non-inductive) and SD conditions.
148 Stem-loop quantitative reverse transcription (qRT) -PCR analysis revealed a reduced
149 accumulation of *miR166* in leaves under SD conditions, while stolons had comparable
150 levels of *miR166* under both the photoperiods (Figure 1F). Stolons differentiating into
151 tubers exhibited 10-40 percent reduction in the later stages of stolon-to-tuber
152 transition (Figure 1G). *In silico* analysis suggested that *miR166* in potato potentially
153 targets six *HD-ZIP III* members, similar to *Arabidopsis*. Using modified 5′ RLM-
154 RACE, we mapped the cleavage site on the HD-ZIP transcripts (Figure 1H),
155 confirming the targets of *miR166*. Overall, our results validate the existence of
156 *miR166-HD-ZIP III* module in potato, and *miR166* showed tissue-specific
157 accumulation under photoperiodic conditions.
158
159 **Knockdown of *microRNA166* causes pleiotropic phenotypic changes**
160 Using a target mimicry approach, we generated stable transgenic lines of *miR166* in *S.*
161 *tuberosum andigena ssp.* (Figure S3A). Of them, 2 independent lines (referred as KD
162 #2 and KD #3) exhibiting 50-75% suppression of mature *miR166* were selected for
163 further characterization (Figure 2A-B). *miR166* KD lines (MIM166) had reduced
164 shoot height but number of nodes remained unchanged, implying a decreased inter-
165 nodal distance, compared to the WT plants (Figure 2C-E). The leaf lamina from
166 *miR166* KD lines appeared flat, hence we calculated the longitudinal and transverse
167 curvature indices (CI^L and CI^T) (Liu *et al*., 2010) to quantify the curvature. A
168 curvature index of zero suggests that the leaf surface is completely flat. Both
169 curvature indices, CI^L and CI^T of the KD lines were significantly reduced compared to

170 WT (Figure 2F-G). The total chlorophyll content in the *miR166* KD lines were
171 comparable to that of WT leaves; and leaves of KD #2 showed a slight increased
172 anthocyanin accumulation, relative to the WT (Figure S3B). The vascular structures
173 were distorted and had fewer xylem elements compared to the WT plants (Figure 2H).
174 Further, an i*n vitro* root growth assay revealed that the MIM166 lines had decreased
175 root length, shoot and root biomass, number of adventitious and lateral roots (Figure
176 S3C-H). Thus, several phenotypic characters were altered upon constitutive and
177 ubiquitous suppression of *miR166* in potato.
178
179 **Suppression of *miR166* alters tuber shape, color and productivity**
180 To examine the effect of *miR166* suppression on tuber development, we subjected the
181 *miR166* KD lines to tuber inductive SD photoperiod in soil conditions. Compared to
182 WT plants, the KD lines showed reduced tuber productivity in varying degrees,
183 although the number of tubers per plant did not vary significantly (Figure 3A-B).
184 Starch estimation assay showed no significant differences in the starch accumulation
185 in tubers of any KD lines, compared to the WT tubers (Figure S3I). Interestingly,
186 tubers from these KD lines were elongated as opposed to the WT spherical tubers
187 (Figure 3C). The sphericity index for these tubers was greater than 1.5, while WT
188 tubers had the sphericity index of around 1.0 (Figure 3D). However, the tuber volume
189 of KD #2 was slightly reduced when compared to WT (Figure 3E). The pigmentation
190 was observed only in the peel of the KD #2 and KD #3 tubers, while the flesh color
191 was comparable to WT (Figure 3C). Metabolic profiling of the tuber peels revealed
192 that KD #2 had increased accumulation of cyanidin 3-glucoside, while KD #3 had
193 increased accumulation of both cyanidin 3-glucoside and pelargonidin 3-glucoside,
194 relative to WT (Figure 3F). In contrast, delphinidin 3-glucoside was reduced in both
195 the KD lines (Figure 3F).
196 *BEL5* and *Identity of Tuber 1* (also known as *BRC1b*) are key positive
197 regulators of tuberization (Chen *et al*., 2003; Tang *et al*., 2022). Relative
198 quantification analyses from stolons of *miR166* KD lines showed a slight reduction in
199 *BEL5* and no significant changes in *IT1* levels (Figure 3G). In potato, SP6A and
200 SWEET11b are crucial for instrumenting symplastic sucrose loading under tuber-
201 inductive conditions (Abelenda *et al*., 2019). *SWEET11b* was found to be significantly
202 reduced in the stolons of both KD lines, along with varying levels of *SP6A* (Figure
203 3G). HY5 binds to the promoters to regulate the expression of *SWEET11* and

204 *SWEET12* in *Arabidopsis* (Chen *et al*., 2016; Sakuraba and Yanagisawa, 2018).
205 Stolons from KD plants had reduced *HY5* levels compared to the WT (Figure 3G).
206 Further, we found that the tuberization potential of these KD lines was greatly
207 reduced (80-100% reduction) under *in vitro* tuber inductive conditions (Figure 3H).
208 Overall, the KD lines exhibited reduced tuberization potential *in vivo* and *in vitro*,
209 accompanied with down regulation of key marker genes.
210

211 **RNA-sequencing analysis revealed differential expression of phytohormone-**
212 **associated genes and accumulation of hormones in swollen *vs*. SSR region of**
213 **tuberizing stolons**

214 The phenotype of elongated and pigmented tuber was evident from the early stages of
215 tuber development (Figure 4A). To identify the genes associated with the tuber
216 phenotype, we carried out paired-end RNA sequencing on two distinct regions-the
217 swollen region (Head) and the sub-swelling region (SSR)-from both WT and KD #3
218 samples (Figure 4B; Figure S4A). The WT_Head and SSR had 37 and 376 uniquely
219 expressed genes respectively, and KD_Head and SSR had 115 and 120 uniquely
220 expressed genes respectively (Figure 4C). A comparison between the Head *vs* SSR
221 tissue revealed 8680 DEGs (4504 up- and 4176-down regulated) in the WT; while
222 7846 DEGs (3830 up- and 4016-down regulated) in the KD samples (Figure S4B-C;
223 Table S1-S2). Using a cut-off of log2 fold change greater than 1 and p-value less than
224 0.05, KD_Head and SSR had 9774 and 10,209 DEGs compared to respective
225 WT_Head and SSR tissues (Figure S4D-E; Table S3-S4).

226 Hormone-related genes showed significant changes in their expression
227 between the Head and SSR tissues from WT and KD (Figure 4D-E; Figure S5A-B).
228 In WT, auxin biosynthesis genes - *StTAA-like*, *StYUCCA4* and *StYUCCA8* were up
229 regulated in the Head compared to the SSR. This spatial expression distinction was
230 lost in the KD line. Also, *StYUCCA5a* and *StYUCCA7* exhibited reversed expression
231 patterns in KD line relative to WT. Auxin transport genes- *StPIN2/4/8/9* displayed
232 markedly altered expression patterns in KD tissues, suggesting perturbed auxin
233 distribution (Figure 4D; Figure S5A). The gibberellin (GA) biosynthesis genes
234 *StGA3ox3* and *StGA20ox2* were found to be up regulated in both the KD tissues
235 (Figure 4D; Figure S5A). Also, the differential expression of the GA catabolic gene
236 *StGA2ox1*, which was evident between Head and SSR in WT, was abolished in the
237 KD line. Expression of the cytokinin (CK) biosynthesis genes *StIPT3/5* and

238 *StCYP735A* was altered and that of *StLOG1a/3b/7c/8b* and *CKX6* in the Head *vs.* SSR
239 tissue was reversed in the KD lines (Figure 4E; Figure S5B). Cytokinin transporter
240 *PUP1-7/9* showed significant reversed expression in the Head *vs.* SSR tissues of
241 respective lines. RT-qPCR analysis of selected phytohormone-related genes validated
242 the RNA-seq results, confirming the altered expression patterns (Figure S5C-D). In
243 line with the transcriptomic data, auxin quantification using LC-MS/MS revealed
244 similar auxin levels in both the Head and SSR regions of KD, whereas WT exhibited
245 significantly lower auxin levels in the SSR (Figure 4F; Data S1.). Additionally, GA_3
246 levels in KD stolons were relatively 5.5 folds lower than those in WT, indicating an
247 altered hormone dynamic in the KD line (Figure 4G).
248 In line with the reduced tuber productivity in MIM lines, positive regulators of
249 tuberization such as *StBEL5* and *StCDF1* were slightly down regulated in KD, relative
250 to WT. *StSWEET11b* levels were greatly reduced in both the KD tissues; while
251 *StSP6A* and *IT1* were specifically down regulated in the SSR region (Figure S6A).
252 RT-qPCR analysis of few marker genes such as *StBEL5*, *StSP6A* and *StHY5*
253 corroborated with the RNA-seq data (Figure S6B-D).
254
255 ***miR166* overexpression exhibits minimal effects on vasculature and tuberization**
256 *MicroRNA166* levels are abundant in the early stolon-to-tuber transitions and decrease
257 at the mini-tuber stage (Figure 1G). To investigate the effects of *miR166*
258 overexpression in potato, we generated stable transgenic lines overexpressing
259 precursor *miR166-d* and evaluated their overall phenotype and tuberization potential
260 under SD conditions. The overexpression (OE) lines OE #9 and #13 lines showed
261 variable levels of mature *miR166* in leaf (Figure S7A-B). OE #13 exhibited a slight
262 reduction in plant height and internodal distance, while the leaf curvature and overall
263 architecture was comparable to those of WT plants (Figure S7C-F). The number of
264 vascular cells in the OE #9 shoot seemed to be increased, relative to the WT plants
265 (Figure S7G). Under SD conditions, the OE #9 exhibited a slight increase in tuber
266 productivity, although the number of tubers remained largely unchanged (Figure S7H-
267 J). RT-qPCR analysis revealed no significant difference in the levels of mature
268 *miR166* in the stolons of OE lines, which may be due to the inherently high *miR166* in
269 the WT stolon (Figure S7K). The tuber marker gene *BEL5* did not show significant
270 variation between OE and WT stolons, while the tuber identity gene *IT1* was up
271 regulated (Figure S7L). Additionally, auxin biosynthesis and transport-related genes

272 were generally up regulated in the stolons of OE lines compared to WT (Figure S7M).
273 Thus, *miR166* OE lines exhibited some phenotypic alterations, comparatively less
274 severe than *miR166* KD lines.
275
276 **REVOLUTA, a *miR166* target affects tuberization**
277 Using modified 5'RLM-RACE, we detected the *miR166* cleaved fragments of *StREV*
278 as predicted by psRNAtarget finder (https://www.zhaolab.org/psRNATarget/home)
279 and mapped the *miR166* cleavage site (Figure 1H; Figure 5A). In the WT stolons,
280 REV transcripts were higher under long-day (LD) conditions and in shoot-forming
281 stolons, whereas SD stolons exhibited dynamic expression across different tissues
282 including the stolon, swollen region, SSR, and mini-tuber (Figure 5B). Stolons from
283 *miR166* KD lines had increased *StREV* levels, while a slight reduction was observed
284 in the OE stolons (Figure 5C). GUS assay of the stable transgenic lines expressing
285 promREV::*uidA* showed promoter activity in the apical and axillary meristems,
286 subtending regions likely corresponding to the vascular tissue, in the swollen regions
287 of tuberizing stolons and at the apex of the mini-tuber stage (Figure 5D). The
288 transcripts of *StREV* were localized in the adaxial side of developing leaves in the
289 shoot apex of WT (Figure 5E). Stable transgenic lines of *StREV* anti-sense (*REV-AS*)
290 exhibited variable degrees of *StREV* suppression in leaves and stolons (Figure S8A-B),
291 however their overall growth and architecture was comparable to WT plants (Figure
292 S8C). The stem vasculature in *StREV* AS #6 was smaller than that of in the WT
293 (Figure S8D). Under SD photoperiod, all three AS lines displayed significantly
294 reduced tuber yield, although the average number of tubers per plant remained largely
295 unchanged (Figure 5F-H). Thus, *REVOLUTA* is a spatio-temporally regulated target
296 of *miR166* in potato, and its suppression led to reduced tuber productivity.
297
298 **StREVOLUTA activates *StYUCCA7***
299 The AT[G/C]AT palindromic sequence was identified as the *in vitro* binding
300 sequence for HD-ZIP III proteins, through which they bind the promoters of auxin-
301 related genes in *Arabidopsis* and regulate their expression (Sessa *et al*., 1998).
302 *REVOLUTA* is known to up regulate the promoter activity of auxin-biosynthesis
303 genes TAA1 and YUCCA5 in Arabidopsis (Brandt *et al*., 2012). Our *in-silico*
304 promoter analysis of auxin biosynthesis genes in potato revealed the presence of these
305 core binding motifs within their upstream regulatory regions, with maximum motifs

being present on the promoter of *StYUCCA7* (Figure 6A). RT-qPCR from the stolons of stable transgenic lines of *StREV* suppression showed reduced accumulation of *StYUCCA* transcripts (Figure 6B), suggesting that the biosynthesis genes could be the targets of StREV. To test this hypothesis, we performed dual-luciferase assay in *Nicotiana benthamiana* leaves. When promoter *StYUC7* was co-infiltrated with *5'm-StREV-FLAG*, the Firefly/Renilla ratios were 10-fold higher that when infiltrated alone, or in presence of an empty vector, suggesting that StREV up-regulated *StYUC7* at the transcriptional level (Figure 6C). To determine whether StREV binds directly to the promoter of *StYUCCA7*, yeast one-hybrid assay was performed. StREV could activate the promoter of *StYUC7* as seen by the robust growth of mated colony on increasing concentrations of 3-AT till 80mM, after which the growth was arrested on higher concentrations (Figure 6D). Thus, StREV could bind to the promoter and up regulate the expression of the auxin biosynthesis gene *StYUCCA7.*

Discussion

Potato is a well-studied model for molecular and hormonal control of tuberization, however, limited knowledge is available on the molecular mechanisms that regulate tuber morphology. In this work, we investigated the role of *miR166* in tuber development in *Solanum tuberosum* spp. *Andigena* 7540. *MiR166* targets six members of the HD-ZIP class III transcription factor family, and is highly expressed in differentiating stolons under SD photoperiod. Suppression of *miR166* led to the pleiotropic effects on overall plant development, particularly affecting tuber shape, color and productivity. Further, StREVOLUTA, a HD-ZIP class III TF regulates auxin biosynthesis during early stolon-to-tuber differentiation *via StYUCCA7.* Our findings identify *miR166*-HD-ZIP III as an important regulator of tuber shape, color and productivity and provides molecular insights about morphology of the storage organ.

The functional roles of *miR166* are conserved in potato

MicroRNAs are key regulators of plant development and defense responses, and amongst them, *miR166* represents a well-conserved family that targets members of the HD-ZIP III transcription factors. Despite the diverse roles attributed to *miR166* in several plants' development, productivity, and stress responses (Ding *et al*., 2013; Zhang *et al*., 2024), its functional characterization in potato and relevance in storage

organ development remains unexplored. In our preliminary analysis of small RNA sequencing datasets (Lakhotia *et al*., 2014; Kondhare *et al*., 2018), we identified *miR166* as the most abundant microRNA in potato stolons, suggesting its involvement in stolon-to-tuber transition stages. A constitutive and ubiquitous knockdown of *miR166* in potato (MIM166) led to the development of several pleiotropic phenotypes. The MIM166 lines had reduced plant height, having no significant changes in the number of nodes (Figure 2C-E). In soybean, Zhao *et al*. (2022) showed that suppression of *miR166* led to decreased plant height. ATHB14-LIKE (a HD-ZIP III TF) promoted the expression of a GA catabolic gene- *GIBBERLLIN 2 OXIDASE2*, causing decreased bioactive GA levels in the plant affecting the height. In potato, MIM166 *in vitro* shoots and roots had increased levels of inactive GA8 (degraded product) and elevated expression of *GA2ox1* in stolons, compared to the WT tissues (Figure S9A-B), suggesting a similar GA dynamics in potato. In *Arabidopsis,* miR165/166 suppression led to pleiotropic effects on leaf development such as trumpet-shaped leaves, ectopic leaflets on the abaxial side, increased leaf numbers and accumulation of purple pigment (Jia *et al*., 2015). Knockdown lines of *miR166* in rice exhibited a rolled-leaf phenotype, having smaller bulliform cells and abnormal sclerenchymatous cells (Zhang *et al*., 2018). In potato, MIM166 lines exhibited reduced curvature of the leaf blades, variations in the total leaflet length and number of lateral leaves (Figure 2F-G; Figure S9C). Thus, *miR166* suppression causes diverse leaf phenotypes in different plants, suggesting a conserved yet species-specific role in regulating leaf development. Two targets of *miR166*, ATHB15 and HB8, play antagonistic roles in the regulation of xylem development in *Arabidopsis* (Baima *et al*., 2001; Kim *et al*., 2005). *ATHB15* is exclusively expressed in vascular tissues and its suppression leads to expanded xylem tissue and inter-fascicular region, indicative of accelerated vascular cell differentiation from cambial/procambial cells (Kim *et al*., 2005). We observed that stable potato transgenic lines of *miR166* (MIM and OE) had altered vascular structures in the stem (Figure 2H; Figure S7G), suggesting *miR166-HD-ZIP III* network might also influence differentiation of vascular cells in potato. Singh *et al*. (2014) showed that phytohormones dynamically regulate the expression of miR165/166 in roots of *Arabidopsis*, and control root meristem size and growth. *In vitro* root growth assay of potato, MIM166 lines showed decreased root length, root biomass, number of adventitious and lateral roots (Figure S3C-H), suggesting the important role of *miR166* in root development of potato. Overall, these pleiotropic

374 phenotypes of the potato MIM166 lines recapitulate the phenotypic traits observed in
375 other plants, and highlight its conserved functional roles as a central regulator of
376 growth and development.
377
378 ***miR166* impacts tuber shape, color, and productivity in potato**
379 Phytohormone quantification, RNA sequencing of tuberizing stolons (Head *vs.* SSR),
380 and anatomical and molecular analyses revealed molecular insights into the altered
381 tuber phenotypes of MIM166 plants. In potato stolons, high GA levels inhibit
382 tuberization, while auxin content increases under inductive conditions. In MIM166
383 stolons, the GA catabolic gene *GA2ox1* was up regulated (Figure 4D), accompanied
384 by a 5.5-fold reduction in bioactive GA_3 (Figure 4G). Genes involved in auxin
385 biosynthesis (*StTAA-like, StYUCCA4/5a/7/8*) and transport (*StPIN2/4/8/9*) showed
386 altered expression in KD_Head *vs*. WT_Head, suggesting disrupted auxin distribution.
387 Consistently, auxin levels in KD Head *vs*. SSR were comparable, unlike the distinct
388 accumulation in WT (Figure 4D). Cytokinin, which is essential for cell division and
389 expansion during tuber bulking (Mingo-Castel *et al*., 1976; Sattelmacher and
390 Marschner, 1978), had reduced expression of its biosynthesis and transport genes in
391 SSR (Figure S5B), affecting the radial cell expansion. Moreover, MIM166 tuber
392 sprouts were stunted, pigmented, and highly branched (Figure S10A), indicating an
393 altered auxin–CK dynamics. We propose that higher auxin in the stalks of developing
394 tubers, altered polar auxin transport, and disrupted auxin–GA–CK balance in the
395 differentiating stolons caused anisotropic expansion leading to elongated tubers in
396 MIM166 plants.
397 Cyanidin 3-glucoside, pelargonidin 3-glucoside, and delphinidin 3-glucoside
398 are water-soluble anthocyanins with strong antioxidant and anti-inflammatory
399 properties (Noda *et al*., 2002; Duarte *et al*., 2018). In our study, MIM166 tubers
400 showed differential accumulation of these pigments in the peel, but not in their flesh
401 (Figure 3C). A similar phenotype was reported in tomato, where overexpression of a
402 petunia chalcone isomerase (CHI) gene increased peel flavonoids by 78-fold without
403 affecting the flesh (Muir *et al*., 2001). In our transcriptomic analysis, we observed an
404 up regulation of multiple structural and accessory genes from the anthocyanin
405 biosynthesis pathway in KD tissues compared to WT, consistent with the increased
406 pigment accumulation (Figure 3F; Figure S10B). Transcription factor families which
407 highly correlated with these pathway genes- bHLH, WRKY, GRAS, bZIP, LBD, ARF,

408 B3, G2-like, HD-ZIP, MYB, and MYB-related also showed significant differential
409 expression (Table S3–S4; Figure S10C). In apple, auxin-induced degradation of
410 MdIAA121 releases MdARF13, which functions as a negative regulator of the
411 anthocyanin biosynthetic pathway (Wang *et al*., 2018). Similarly, auxin suppresses
412 anthocyanin accumulation by promoting the degradation of MdIAA26 (Wang *et al*.,
413 2020). In potato, tuberizing stolons have high auxin levels. We speculate that this high
414 auxin could have restricted pigment accumulation to the tuber peel in the MIM166
415 lines, thereby resulting pigmented peels but non-pigmented tuber flesh. Conversely,
416 flavonoids have been reported to act as inhibitors of auxin transport (Gayomba *et al*.,
417 2016), which may have altered auxin distribution in the KD stolons. Further studies
418 are required to ascertain how auxin dynamics in tuberizing stolons influence
419 anthocyanin accumulation and, consequently, tuber morphology.
420 Under tuber inductive SD photoperiod, SWEET11b- SP6A interacts to
421 mediate the symplastic loading of sucrose, and prevents its loss to the apoplastic route
422 (Abelenda *et al*., 2019). MIM166 plants showed strong reduction in SWEET11b
423 levels (Figure 3G; Figure S6A), and had distorted vascular structures (Figure 2H),
424 both of which could have contributed to impaired sucrose transport causing reduced
425 tuber productivity, while not significantly affecting the starch content per gram fresh
426 weight of the tuber (Figure 3A; Figure S3I). Interestingly, MIM166 plants developed
427 floral buds at the shoot apex and aerial stolon/tubers under SD photoperiod (Figure
428 S11A-C), denoting the formation of ectopic sinks due to the improper sucrose
429 distribution and/or cytokinin metabolism. As SD induction progressed, the
430 belowground developing tubers acted as the primary and stronger sinks, thus limiting
431 sucrose availability for the ectopic sinks leading to floral bud abortion. Thus, the
432 reduced belowground tuber productivity could be a cumulative effect of altered
433 vascular structures, improper symplastic loading of sucrose, and impaired tuber-
434 bulking at the stolon apex due to the disrupted phytohormone dynamics.
435
436 ***MiR166*-Revoluta-auxin: Role in tuberization**
437 Auxin plays a key role in the stolon-to-tuber transition process. The stolon apical
438 meristem (StAM) is a major site of auxin biosynthesis, where YUC-like1 (*StYUC4*)
439 acts as a key contributor (Roumeliotis *et al*., 2012). In *Arabidopsis*, REVOLUTA
440 regulates promoters of auxin biosynthesis, transport, and signaling genes (Brandt *et*
441 *al*., 2012; Reinhart *et al*., 2013). In our study, phenotypes such as impaired root

442 growth, increased tuber sprout branching, and altered auxin-related gene expression
443 suggested a role for REVOLUTA in potato (Figure 5A–C; Figure S3C-H; Figure
444 S10A). Through GUS assay, we observed that the promoter activity of *StREV* was
445 visible in the stolon apex, vascular region and subsequent tuberizing stages (Figure
446 5D). This was similar to the activity of an auxin responsive promoter *DR5:GUS*
447 observed by Roumeliotis *et al*. (2012), suggesting a putative overlap of *StREV*
448 expression and auxin accumulation. *StREV* antisense (REV-AS) lines exhibited
449 reduced tuber yield (Figure 5F-H). Also, StREV could bind to the promoter of
450 *StYUC7* and activate its expression (Figure 6D-E). These findings suggest a hitherto
451 unknown role of REV in tuberization, probably through auxin.

452 We propose a model for the *miR166*–REV–auxin regulatory module in
453 influencing tuber shape and size in potato (Figure 7). In WT, high levels of *miR166* in
454 stolons fine tune the expression of *StREV*. This leads to a balanced metabolism of
455 auxin in the tuberizing stolons, resulting in isotropic expansion and formation of
456 spherical tubers. In the MIM166 lines, suppression of *miR166* caused increased and/or
457 ectopic expression of *StREV*. This altered the auxin biosynthesis, and polar auxin
458 transport, causing anisotropic expansion of the stolons and forming elongated tubers.
459 In the *REV-AS* lines, lower levels of *StREV* affected auxin biosynthesis, and resulted
460 in reduced tuber size and lower productivity compared to the WT. Collectively, these
461 findings support a model, wherein the *miR166*–REV–auxin regulatory module
462 governs auxin biosynthesis during stolon differentiation, thereby influencing tuber
463 morphology (Figure 7). Given that auxin levels are highly dynamic during
464 tuberization, further studies are needed to elucidate the spatio-temporal regulation of
465 the *miR166*–REV and its impact on auxin synthesis/transport. Additionally, members
466 of the HD-ZIP III TF family could also play a role in the stolon-to-tuber transitions
467 and needs further investigations (Figure S12A-B).

468 Our transcriptomic datasets revealed that genes located within QTL regions on
469 chromosomes 5, 10, and 12- associated with tuber shape and eye depth- were
470 differentially expressed (Figure S13A; Tables S3–S4). Though we do not see a
471 marked difference in the *StOFP20* expression (Ju *et al*., 2023); differential expression
472 of 19 other OFPs suggests the involvement of more than one OFP genes in
473 influencing tuber shape (Figure S13B). Additionally, several genes within the *Ro*
474 locus (Fan *et al*., 2022) were down regulated in KD_Head compared to WT_Head

475 (Figure S13C; Table S3). Further studies of these genes will elucidate their role(s) in
476 determining tuber morphology.
477 Tuber morphology is shaped by the coordinated interplay of phytohormone
478 and developmental gene regulatory networks that govern cell division, expansion, and
479 tissue organization. Although the *miR166*-HD-ZIP III module is widely associated
480 with adaxial-abaxial polarity in dorsiventral lateral organs, our findings uncover its
481 functional relevance in a radially symmetric storage organ. We demonstrate that this
482 regulatory module contributes to tuber development by modulating auxin-associated
483 pathways, with REVOLUTA regulating auxin biosynthesis genes and influencing
484 tuberization. Further studies in functional diversification of HD-ZIP III members will
485 provide insights into how small RNA-transcription factors can fine-tune organ
486 architecture in diverse developmental contexts.
487
488 **Materials and Methods**
489
490 **Plant material and growth conditions**
491 A photoperiod-responsive potato cultivar *Solanum tuberosum* ssp. *andigena* 7540
492 which tuberizes under SD conditions, was used in this study. *In vitro* plants (wild-type
493 and transgenic lines) were propagated from axillary node sub-cultures on Murashige
494 and Skoog's basal medium with 2% (w/v) sucrose (Murashige and Skoog., 1962) and
495 were grown in a plant growth incubator (Percival Scientific, Inc.) with a light
496 intensity of 300 μmol m−2 s−1 under LD conditions unless mentioned otherwise.
497
498 **Prediction and detection of *miR166* precursors in potato**
499 Four precursor sequences (stu-*MIR166*a, stu-*MIR166*b, stu-*MIR166*c and stu-
500 *MIR166*d) of *miR166* were retrieved from the miRBase (http://mirbase.org/; Griffiths-
501 Jones S *et al*., 2008). The secondary structures of these precursors were predicted
502 using the Mfold software (http://www.unafold.org/mfold/applications/rna-folding-
503 form.php; Zuker, 2003), and structures with lowest free energies were then further
504 screened for having the characteristic stem-loop secondary structure with the mature
505 miRNA sequence in the arm region of the stem-loop. All four miRNA precursors
506 were then validated from *S. tuberosum* ssp. *andigena* 7540 by RT-PCR analysis. The
507 sequences of all the oligos used in this study are provided in Table S5, and the IDs for
508 all the genes are in the Table S6.

509 Total RNA was harvested from shoot apex, mature leaves and stolon tissues of
510 potato using RNAiso Plus (DSS TAKARA) as per the manufacturer's instructions.
511 cDNA was synthesized using two microgram (2µg) of total RNA, Superscript IV
512 Reverse Transcriptase (Invitrogen), and oligo dT primers. miRNA precursors were
513 amplified by RT-PCR using precursor-specific primer pairs. The amplicons were
514 cloned into sub-cloning vector pGEMT-easy (Promega) and sequence verified.
515
516 **Validation of mature *miR166***
517 Total RNA was isolated using RNAiso Plus (DSS TAKARA) from mature leaves and
518 stolons of WT potato plants. One microgram (1 µg) of total RNA was used for cDNA
519 preparation using *miR166* specific stem-loop primers (STP) followed by their end-
520 point PCRs using *miR166* specific forward and universal reverse primer as described
521 in Varkonyi-Gasic *et al*. (2007) (Table S5).
522
523 **Tissue-specific relative abundance of *miR166* under SD and LD conditions**
524 For investigating the influence of photoperiod on tissue-specific accumulation of
525 mature *miR166*, *in vitro* grown wild-type *S. tuberosum* spp. *andigena* 7540 plants
526 were transferred to soil and maintained under LD photoperiod with 300 µmol m−2
527 s−1 light intensity for a period of ten weeks (until they attained 10-12 leaf stages) in a
528 growth chamber (Percival Scientific, Inc.). Later, half of the plants were transferred to
529 tuber-inductive SD photoperiod for 7 days, while the remaining plants were
530 maintained under LD conditions. Leaves and stages of stolon-to-tuber transitions were
531 collected at 7 days post LD/SD induction in triplicates. Isolation of total RNA and
532 cDNA synthesis was carried out as described before. qPCR reactions were performed
533 on CFX96 Real-Time System (BIO-RAD) with *miR166*-specific forward primer and
534 universal reverse primer, using TAKARA SYBR green master mix (Takara-Clontech).
535 The reaction mix was incubated at 95 °C for 30 s, followed by 40 cycles at 95 °C for
536 5 s, gene-specific annealing temperature for 15 s and extension for 72 °C for 15 s.
537 PCR specificity was checked by melting curve analysis, and data were analyzed using
538 the $2^{-\Delta\Delta Ct}$ method (Livak and Schmittgen, 2001).
539
540 **Generation of constructs and potato transgenic lines**
541 MicroRNA166 overexpression (OE) and mimicry (MIM) constructs for
542 overexpression and suppression of the *miR166*, respectively, were previously

543 generated in our lab. Briefly, *miR166* OE construct- 35S:St-pre166D-pBI121 was
544 generated by amplifying precursor (St-pre166-d) from potato RNA using primers
545 Pre166d-FP and Pre166d-RP (Table S5). The amplified product (108 bp) was cloned
546 into the binary vector pBI121 downstream to the 35S CaMV constitutive promoter.
547 For knockdown (KD) construct, we used artificial target mimicry (MIM) strategy.
548 The KD construct (originally in pGREEN vector) was obtained from European
549 *Arabidopsis* Stock Centre (NASC) (Todesco *et al*., 2010), and the MIM166 insert
550 (542 bp) was re-cloned to pBI121 binary vector to generate 35S:MIM166-pBI121.
551 Both these constructs- OE and MIM were then mobilized into *Agrobacterium*
552 *tumefaciens* strain GV3101. Transgenic potato plants in *S. tuberosum* spp. *andigena*
553 7540 were generated as described in Banerjee *et al*., 2006. Kanamycin-resistant
554 transgenic plants were further screened by molecular methods and selective lines were
555 used for further experiments.
556 After 4 weeks of *in vitro* growth, potato plants were transferred to soil, grown
557 for 7-9 weeks under LD conditions, before initiating SD induction. Phenotypic
558 characteristics such as plant height, number of nodes and leaf curvature were recorded
559 just before the initiation of SD photoperiod treatment, whereas the frequency of floral
560 bud formation and tuber productivity parameters were measured after 1 and 8-9 weeks
561 of SD induction, respectively.
562
563 **Phenotypic analysis**
564 All the phenotypic analyses were performed on 6–7 weeks old soil-grown plants.
565 Shoot height was measured from the bottom-most node up to the plant apex. For
566 measurement of leaf curvature indices, mature terminal leaves at the fifth node were
567 analyzed as described in Liu *et al*., 2010. These experiments were performed at least
568 three times with similar results.
569
570 **Assessment of tuber productivity**
571 One-month-old plantlets of the transgenic lines and WT were transferred to soil in
572 small round pots and hardened for one week under LD conditions in a growth
573 chamber (Percival Scientific, Inc.) with a light intensity of 300 μmol m−2 s−1, day
574 temperature of 24°C, and night temperature of 22°C. This was followed by an
575 additional three weeks of incubation in the same pots. Subsequently, the plants were
576 re-potted into medium-sized pots and continued to grow under LD conditions for an

577 additional five weeks. When the plants reached the 10-12 leaf stage, they were
578 transferred to tuber inductive short-day (SD) conditions (16h dark and 8h light) with
579 day and night temperatures of 22°C and 20°C, respectively. A subset of these plants
580 was harvested after 7 days of induction, and stolons were collected for RT-qPCR
581 analysis. After 60 days of induction, remaining plants were evaluated for their tuber
582 productivity (gram fresh weight [g fr wt] per plant) and tuber numbers. This
583 experiment was carried out 3 times, with consistent results. For tuber sphericity index
584 and volume assessment, 30 tubers per line were measured for their diameters
585 (Diameter1, Diameter2 and height). *In vitro* tuber induction assay was performed
586 (experiment was repeated three times independently) as described in Kondhare *et al*.,
587 2021.
588
589 **Starch estimation**
590 Starch estimation was carried out twice, independently, as described in Kamble *et al*.
591 (2023), Hawkins *et al*. (2021) and Kringel *et al*. (2020), with minor modifications.
592 Tuber tissue was well-homogenized in cold water containing 0.35% sodium
593 metabisulphte. The slurry was filtered to remove the debris. Filtered solution was kept
594 undisturbed for 1 hour at 4 degrees. Insoluble material was collected by centrifugation,
595 followed by 3 washes with 80% ethanol, and then finally re-suspended in water.
596 Starch was digested using alpha amylase (SRL), glucoamylase (SRL) and
597 Amyloglucosidase (Sigma). Glucose was estimated using the DNSA method, and
598 compared with a standard graph prepared using Starch (Sigma), digested under
599 identical conditions.
600
601 **RNA sequencing**
602 For RNA-sequencing, *miR166* KD #3 and WT plants were grown in soil for 10-weeks
603 under LD conditions and subjected to SD induction for 12 days. Swollen stolons were
604 harvested in triplicates (from at least 20 plants per replicate) and divided into swelling
605 (Head) and sub-swelling region (SSR) and snap-frozen in liquid nitrogen. The tissues
606 were crushed using liquid Nitrogen and stored in -80º C until further use. For RNA
607 sequencing and RT-qPCR purposes, 100 mg of tissue from each sample was used to
608 isolate the total RNA using RNAiso Plus as per the manufacturer's instructions. RNA
609 quality and integrity were assessed, and RNA-sequencing was performed by
610 Novelgene Technologies Pvt. Ltd., Hyderabad. Paired-end sequencing was performed

611 on Illumina NovaSeq 6000, adapter sequences and low-quality reads were filtered
612 using FASTP to get high-quality reads on the parameter of <Q20, length < 50. Further
613 processing was performed as described in Kumar *et al*. 2020. Validation of selected
614 target genes identified in the RNA-seq analysis was done using qPCR as described
615 above.
616
617 **Detection of phytohormones and pigments by LC-MS/MS**
618 Tissues- stolon, swollen stolon (Head and SSR), tuber peel, tuber flesh were harvested,
619 crushed in liquid Nitrogen, and stored at -80º C until further use. 100 mg of the
620 crushed powder was extracted with 1 ml of extraction solvent (For phytohormone
621 extraction- MS grade methanol/water/formic acid 75:20:5; having 300ng internal
622 standard Adonitol; For pigment extraction- 80 percent methanol in MS grade water;
623 having 300ng internal standard Adonitol), by 3-5 min of vigorous vortex, followed by
624 15 min of sonication. The solution was incubated overnight at -80°C under dark
625 conditions. Next day, the samples were centrifuged at 4°C, maximum speed for 15
626 min. The supernatant was transferred into a new tube, and reduced to half of its
627 original volume, using centrivap at 4°C, and was filtered through 0.22-micron syringe
628 filter. The LC-MS system (Exion AD, AB Sciex) was used for detection of
629 phytohormones and pigments. Chromatographic separation was done on AB SCIEX
630 Exion LC AD UPLC system, using Phenomenex kinetex core shell C18 column
631 (2.1X150 mm, 1.7µm). Separation of compounds was performed at 0.3 ml/ min flow
632 rate with linear gradient of solvent A (milliQ + 0.1% formic acid) and solvent B
633 (Acetonitrile + 0.1% formic acid) was performed as follows: 0 min 5% B + 95% A; 3
634 min, 10% B; 6 min, 50% B, 7 min, 70% B; 10 min, 95% B; 12 min, finally column
635 was re-equilibrated to initial ratio of 5% B + 95% A for 4 min with total run time of
636 16 min. The m/z range for phytohormone and pigment detection was 100-400 and
637 100-1700, respectively. The sample injection volume was 40 µl for all the samples.
638 Three blank runs were given every time between the biological replicates throughout
639 run. The full scan mass spectrometry data was acquired on the X500R Q-TOF (AB
640 Sciex, USA). The data for all the samples were acquired using electrospray ionization
641 in both positive and negative modes. Mass calibration was performed in positive and
642 negative ion modes before the data acquisition. Data analysis was carried out using
643 the SCIEX OX software provided along with the machine.
644

645 **GUS assay**

646 *StREV* promoter transgenic lines (promREV:*uidA*) were grown *in vitro* under LD
647 conditions for 20 d. They were also grown in soil under LD conditions for 8 weeks,
648 followed by SD induction for 15 d. Entire *in vitro* grown plantlets, stolon and tuber
649 samples from SD-induced soil-grown plants were subjected to GUS assay as
650 described in Begum *et al*., (2022) and imaged using olympus MX stereozoom
651 microscope.

652

653 **RNA *insitu* hybridization**

654 Longitudinal sections of 8 µm thickness from shoot apex of WT plants were probed
655 with digoxigenin (DIG)-labeled antisense mRNA probes. The probes to detect *StREV*
656 transcripts were PCR- amplified from cDNA using specific primer pairs (Table S5)
657 that amplify part of the cDNA, with T7 RNA polymerase binding site attached to the
658 reverse primer and forward primer. Two independent clones in distinct orientations
659 were used to synthesize the respective sense and anti-sense probes. RNA *insitu*
660 hybridization was carried out as described by Abelenda *et al*., 2019.

661

662 **Chlorophyll and anthocyanin estimation**

663 Anthocyanin and chlorophyll estimation from leaves of WT and *miR166* KD lines
664 was performed as per the method in Nakata and Ohme-Takagi (2014) and
665 Bhattacharjee and Sharma (2012), respectively. These experiments were conducted
666 two times, with similar results.

667

668 **Histology**

669 For anatomical studies, stems from the middle part of soil-grown plants (6 weeks LD)
670 were used. Free hand transverse sections were cut using a sharp razor blade, and
671 selective sections were stained with Toluidine Blue O solution as described in
672 Pradhan Mitra and Loqué., 2014. The sections were mounted in 70% glycerol, before
673 imaging them on the Nikon Eclipse microscope.

674

675 **Dual-luciferase assay**

676 The promoter of *StYUC7* was cloned in the pGreenII0800-LUC vector upstream of
677 the LUC gene. The coding sequence of *5'm-StREV-FLAG* (*StREV* resistant to *miR166*)
678 was cloned in pCB201 downstream to the cauliflower mosaic virus 35S promoter.

679 Both the constructs were transformed in *A. tumefaciens* strain GV3101. The promoter
680 *StYUC* in pGreenII0800-LUC was co-infiltrated in leaves of *N. benthamiana* with the
681 *5'm-StREV-FLAG* or a negative control empty vector pCB201. Twelve bioreplicates
682 were collected for each condition after 48 hours post-infiltration. Firefly and Renilla
683 luciferase activities were measured using the Dual-Luciferase Reporter Assay System
684 (Promega).
685
686 **Yeast-one hybrid assay**
687 The coding sequence of *StREV* and the promoter sequence of *StYUCCA7* (~3.0 kb
688 upstream) were cloned into the pGEM-T Easy vector (Promega). For preparation of
689 bait expression vector, the promoter was cloned in the destination vector pMW#2
690 (Addgene) through the restriction sites MluI and SacII. The yeast strain YM4271 was
691 transformed with this bait expression vector (linearised) containing promoter of
692 *StYUC7* and selected in SD-His medium. The prey expression vector was prepared by
693 transferring the coding sequence of *StREV* to the destination vector pDEST-2μ-Gal4-
694 AD via the donor vector pDONR221. The yeast strain Yα1867 was transformed with
695 the prey expression vector and selected in SD-Trp medium. To study the interaction,
696 the prey yeast (Yα1867-StREV) and the bait yeast (YM4271-prom-StYUC7) were
697 mated by mixing in a 1:1 ratio and allowed to grow in YPDA medium. The mated
698 yeast clones were then selected on SD -His, -Trp medium. The interaction was further
699 confirmed by growing the mated yeast clones on SD -His, -Trp medium supplemented
700 with increasing concentrations of 3-amino-1,2,4-triazole (3-AT).
701
702 **Data availability**
703 The raw sequencing data were deposited in the NCBI Short Read Archive (SRA)
704 database (http://www.ncbi.nlm.nih. gov/sra/). It can be retrieved using the SRA ID
705 SRP630954. All other relevant data can be found within the manuscript and its
706 supporting materials.
707
708 **Acknowledgements**
709 Authors acknowledge Mr. Nilesh Lohakare and Mr. Nitish Lahigude (Indian Institute
710 of Science Education and Research, Pune) for their help in maintaining the plants in
711 the green house facility. We thank Novelgene Technologies Pvt. Ltd. for performing
712 RNA sequencing. We are grateful to Ms. Drishti Kataria (IISER Pune) for her

assistance in screening the Y1H clones. We are thankful to Dr. Harpreet Singh Kalsi, Dr. Nilam Malankar, Dr. Kirtikumar Kondhare and Ms. Shikha Singh for their inputs. The authors used ChatGPT (OpenAI) exclusively for language editing and grammar refinement. The scientific content, interpretation, and conclusions are solely those of the authors.

Funding

NSP and JK are thankful to the University Grants Commission for the Senior Research Fellowship and Junior Research Fellowship, respectively. GA acknowledges funding received from the Department of Biotechnology, India. AKB acknowledges the support and generous funding from the Indian Institute of Science Education and Research (IISER) Pune.

Authors contributions

N.S.P. designed the experiments, generated transgenic lines, carried out phenotypic and transcriptomic data analyses, conducted experiments and wrote the manuscript draft. A.V. conducted the LC-MS/MS experiments and analyzed its data. B.N. and N.S.P. performed RLM-RACE for target validation. G.A. and N.S.P. generated the *miR166* KD and promREV::uidA transgenic lines. J.K. assisted in molecular cloning and analysis. A.K.B. supervised the study, obtained the funding and resources. N.S.P. and A.K.B. conceived the idea and edited the manuscript. All authors have read and approved the final manuscript.

Conflict of Interest Statement

The authors declare that they have no conflicts of interest associated with this work.

Ethics Statement

All experimental research on plants in this study complied with institutional bio-safety guidelines. The plant materials used were maintained in accordance with relevant regulations.

Supporting Information

Figure S1. Details of the precursors and mature *miR166* in potato

746 **Figure S2.** Abundance of *miR166* in stolons under early LD *vs* SD stages from a
747 photoperiod dependent tuberizing variety ssp. *andigena* 7540
748 **Figure S3.** Pleiotropic phenotypes of *miR166* suppression on potato
749 **Figure S4.** PCA and Volcano plots of samples processed for RNA-sequencing
750 **Figure S5.** Heatmap and RT-qPCR for selective phytohormone genes
751 **Figure S6.** Heatmap and RT-qPCR for selective tuberization genes
752 **Figure S7.** Characterization of the *miR166* OE lines
753 **Figure S8.** Characterization of the REV AS lines
754 **Figure S9.** GA8 quantification from *in vitro miR166* KD plants
755 **Figure S10.** Tuber sprout phenotype and heat map for anthocyanin-related genes
756 **Figure S11.** Development of ectopic sinks in *miR166* KD lines under SD photoperiod
757 **Figure S12.** Heat maps for selective QTL genes
758 **Figure S13.** Relative fold change of the *HD-ZIP class III* transcripts
759
760 **Supporting Tables**
761 **Table S1.** Differentially expressed genes in WT_Head compared to WT_SSR
762 **Table S2.** Differentially expressed genes in KD_Head compared to KD_SSR
763 **Table S3.** Differentially expressed genes in KD_Head compared to WT_Head
764 **Table S4.** Differentially expressed genes in KD_SSR compared to WT_SSR
765 **TableS5.** List of Primers
766 **Table S6.** List of gene IDs
767
768 **Supporting Data S1.** MS-MS fragment match for phytohormones and pigments
769
770 **References**

771 • Abelenda JA, Bergonzi S, Oortwijn M, Sonnewald S, Du M, Visser RGF,
772 Sonnewald U, Bachem CWB. 2019. Source-sink regulation is mediated by
773 interaction of an FT homolog with a SWEET protein in potato. Curr Biol.
774 29:1178–1186.e6. doi:10.1016/j.cub.2019.02.018
775 • Baima S, Possenti M, Matteucci A, Wisman E, Altamura MM, Ruberti I,
776 Morelli G. 2001. The Arabidopsis ATHB-8 HD-Zip protein acts as a
777 differentiation-promoting transcription factor of the vascular meristems. Plant
778 Physiol.

- Banerjee AK, Prat S, Hannapel DJ. 2006. Efficient production of transgenic potato (S. tuberosum L. ssp. andigena) plants via Agrobacterium tumefaciens-mediated transformation. Plant Sci. 170:732–738. doi:10.1016/j.plantsci.2005.11.007
- Begum S, Jing S, Yu L, Sun X, Wang E, Abu Kawochar M, Qin J, Liu J, Song B. 2022. Modulation of JA signalling reveals the influence of StJAZ1-like on tuber initiation and tuber bulking in potato. Plant J. 109:952–964. doi:10.1111/tpj.15606
- Bhattacharjee S, Sharma GD. 2012. Effect of dual inoculation of arbuscular mycorrhiza and rhizobium on the chlorophyll, nitrogen and phosphorus contents of pigeon pea (Cajanus cajan L.). Adv Microb. 2:25945. doi:10.4236/aim.2012.24072
- Brandt R, Salla-Martret M, Bou-Torrent J, Musielak T, Stahl M, Lanz C, Ott F, Schmid M, Greb T, Schwarz M, Choi SB, Barton MK, Reinhart BJ, Liu T, Quint M, Palauqui JC, Martínez-García JF, Wenkel S. 2012. Genome-wide binding-site analysis of REVOLUTA reveals a link between leaf patterning and light-mediated growth responses. Plant J. 72:31–42. doi:10.1111/j.1365-313X.2012.05049.x
- Bu, H., Sun, X., Hu, Y., Gu, G., Yang, Y., & Yu, W. (2025). Research advances in the regulation of fruit size: An integrated perspective of genetic, hormonal, epigenetic, and environmental control. Biology, 14(12), 1643. https://doi.org/10.3390/biology14121643
- Che, R., Tong, H., Shi, B., Liu, Y., Fang, S., Liu, D., Xiao, Y., Wang, H., Liu, L., & Wang, C. (2016). Control of grain size and rice yield by GL2-mediated brassinosteroid responses. Nature Plants, 2, 15195. https://doi.org/10.1038/nplants2015195
- Chen H, Rosin FM, Prat S, Hannapel DJ. 2003. Interacting transcription factors from the three-amino acid loop extension superclass regulate tuber formation. Plant Physiol. 132:1391–1404. doi:10.1104/pp.103.022434
- Chen S, Wang XJ, Tan GF, Zhou WQ, Wang GL. 2020. Gibberellin and the plant growth retardant paclobutrazol altered fruit shape and ripening in tomato. Protoplasma. 257:853–861. doi:10.1007/s00709-019-01471-2

811 • Chen X, Yao Q, Gao X, Jiang C, Harberd NP, Fu X. 2016. Shoot-to-root
812 mobile transcription factor HY5 coordinates plant carbon and nitrogen
813 acquisition. Curr Biol. 26:640–646.
814 • Ding, Y., Tao, Y., & Zhu, C. (2013). Emerging roles of microRNAs in the
815 mediation of drought stress response in plants. Journal of Experimental
816 Botany, 64(11), 3077–3086. https://doi.org/10.1093/jxb/ert164
817 • Duarte LJ, Chaves VC, Nascimento MVP dos S, Calvete E, Li M, Ciraolo E,
818 Ghigo A, Hirsch E, Simões CMO, Reginatto FH, Dalmarco EM. 2018.
819 Molecular mechanism of action of pelargonidin-3-O-glucoside, the main
820 anthocyanin responsible for the anti-inflammatory effect of strawberry fruits.
821 Food Chem. 247:56–65. doi:10.1016/j.foodchem.2017.12.015
822 • Eldridge, T., Łangowski, Ł., Stacey, N., Jantzen, F., Moubayidin, L., Sicard,
823 A., Southam, P., Kennaway, R., Lenhard, M., Coen, E. S., & Østergaard, L.
824 (2016). Fruit shape diversity in the Brassicaceae is generated by varying
825 patterns of anisotropy. Development, 143(18), 3394–3406.
826 https://doi.org/10.1242/dev.135327
827 • Fan G, Wang Q, Xu J, Chen N, Zhu W, Duan S, Yang X, De Jong WS, Guo Y,
828 Jin L, Li G. 2022. Fine mapping and candidate gene prediction of tuber shape
829 controlling Ro locus based on integrating genetic and transcriptomic analyses
830 in potato. Int J Mol Sci. 23:1470. doi:10.3390/ijms23031470
831 • Fan, C., Xing, Y., Mao, H., Lu, T., Han, B., Xu, C., Li, X., & Zhang, Q.
832 (2006). GS3, a major QTL for grain length and weight and minor QTL for
833 grain width and thickness in rice, encodes a putative transmembrane protein.
834 Theoretical and Applied Genetics, 112(6), 1164–1171.
835 https://doi.org/10.1007/s00122-006-0218-1
836 • Gayomba, S. R., Watkins, J. M., & Muday, G. K. (2016). Flavonols regulate
837 plant growth and development through regulation of auxin transport and
838 cellular redox status. In K. Yoshida, V. Cheynier, & S. Quideau (Eds.), Recent
839 Advances in Polyphenol Research (Vol. 5, pp. 143–170). John Wiley & Sons.
840 https://doi.org/10.1002/9781118883303.ch7
841 • Griffiths-Jones S, Saini HK, van Dongen S, Enright AJ. 2008. miRBase: tools
842 for microRNA genomics. Nucleic Acids Res. 36:D154–D158.

843 • Hawkins E, Chen J, Watson-Lazowski A, Ahn-Jarvis J, Barclay JE, Fahy B,
844 Hartley M, Warren FJ, Seung D. 2021. STARCH SYNTHASE 4 is required
845 for normal starch granule initiation in amyloplasts of wheat endosperm. New
846 Phytol. 230:2371–2386. doi:10.1111/nph.17342
847 • Hu, J., Fan, J., Sun, C., & Tang, H. (2012). OsPPKL1, a protein phosphatase
848 with Kelch-like repeat domains, affects grain length in rice. Plant Cell Reports,
849 31(3), 509–519. https://doi.org/10.1007/s00299-011-1168-0
850 • Hu, J., Liu, H., Li, Y., Liu, H., & Duan, P. (2015). OsGRF4 and OsGIF1
851 regulate rice grain shape through controlling cell expansion. Plant
852 Biotechnology Journal, 13(6), 849–859. https://doi.org/10.1111/pbi.12341
853 • Jia X, Ding N, Fan W, Yan J, Gu Y, Tang X, Li R, Tang G. 2015. Functional
854 plasticity of miR165/166 in plant development revealed by small tandem
855 target mimic. Plant Sci. 233:11–21. doi:10.1016/j.plantsci.2014.12.020
856 • Ju A, Wang Y, Yan Y, Li C, Luo W, Ma L, Shang Y, Gao D. 2023. StOFP20
857 regulates tuber shape and interacts with TONNEAU1 recruiting motif proteins
858 in potato. J Integr Agric. 22:752–761. doi:10.1016/j.jia.2022.08.069
859 • Kamble UN, Makhamadjonov F, Fahy B, Martins C, Saalbach G, Seung D.
860 2023. Initiation of B-type starch granules in wheat endosperm requires the
861 plastidial α-glucan phosphorylase PHS1. Plant Cell. 35:4091–4110.
862 doi:10.1093/plcell/koad217
863 • Kim J, Jung JH, Reyes JL, Kim YS, Kim SY, Chung KS, Kim JA, Lee M, Lee
864 Y, Kim VN, Chua NH, Park CM. 2005. microRNA-directed cleavage of
865 ATHB15 mRNA regulates vascular development in Arabidopsis inflorescence
866 stems. Plant J. 42:84–94. doi:10.1111/j.1365-313X.2005.02354.x
867 • Kondhare KR, Kumar A, Patil NS, Malankar N, Saha K, Banerjee AK. 2021.
868 Development of aerial and belowground tubers in potato is governed by
869 photoperiod and epigenetic mechanism. Plant Physiol. 187:1071–1086.
870 doi:10.1093/plphys/kiab409
871 • Kondhare KR, Malankar NN, Devani RS, Banerjee AK. 2018. Genome-wide
872 transcriptome analysis reveals small RNA profiles involved in early stages of
873 stolon-to-tuber transitions in potato under photoperiodic conditions. 1–19.
874 • Kringel DH, el Halal SLM, Zavareze Eda R, Dias ARG. 2020. Methods for
875 the extraction of roots, tubers, pulses, pseudocereals, and other unconventional

876 starch sources: a review. Starch/Staerke. 72:11–12.
877 doi:10.1002/star.201900234

- 878 Kumar A, Kondhare KR, Vetal PV, Banerjee AK. 2020. PcG proteins MSI1
879 and BMI1 function upstream of miR156 to regulate aerial tuber formation in
880 potato. Plant Physiol. 182:185–203. doi:10.1104/pp.19.00416
- 881 Lakhotia N, Joshi G, Bhardwaj AR, Katiyar-Agarwal S, Agarwal M,
882 Jagannath A, Goel S, Kumar A. 2014. Identification and characterization of
883 miRNAome in root, stem, leaf and tuber developmental stages of potato
884 (Solanum tuberosum L.) by high-throughput sequencing. BMC Plant Biol.
885 14:6.
- 886 Li, S., Li, H., Ye, G., et al. (2016). The OsmiR396c-OsGRF4-OsGIF1
887 regulatory module determines grain size and yield in rice. Plant Biotechnology
888 Journal, 14(11), 2134–2146. https://doi.org/10.1111/pbi.12569
- 889 Lindqvist-Kreuze H, Khan A, Salas E, Meiyalaghan S, Thomson S, Gomez R,
890 Bonierbale M. 2015. Tuber shape and eye depth variation in a diploid family
891 of Andean potatoes. BMC Genet. 16:57. doi:10.1186/s12863-015-0213-0
- 892 Liu Z, Jia L, Mao Y, He Y. 2010. Classification and quantification of leaf
893 curvature. J Exp Bot. 61:2757–2767. doi:10.1093/jxb/erq111
- 894 Liu, J., Van Eck, J., Cong, B., & Tanksley, S. D. (2002). A new class of
895 regulatory genes underlying the cause of pear-shaped tomato fruit. Science,
896 296(5565), 343–346. https://doi.org/10.1126/science.1068759
- 897 Livak KJ, Schmittgen TD. 2001. Analysis of relative gene expression data
898 using real-time quantitative PCR and the 2(-ΔΔC(T)) method. Methods.
899 25:402–408.
- 900 Mao, H., Sun, S., Yao, J., Wang, C., Yu, S., Xu, C., Li, X., & Zhang, Q.
901 (2010). Linking differential domain functions of the GS3 protein to natural
902 variation of grain size in rice. Proceedings of the National Academy of
903 Sciences of the United States of America, 107(45), 19579–19584.
904 https://doi.org/10.1073/pnas.1014415107
- 905 Mingo-Castel AM, Young RE, Smith OE. 1976. Kinetin-induced tuberization
906 of potato in vitro: on the mode of action of kinetin. Plant Cell Physiol. 17:557–
907 567.

908 • Muir S, Collins G, Robinson S, et al. 2001. Overexpression of petunia
909 chalcone isomerase in tomato results in fruit containing increased levels of
910 flavonols. Nat Biotechnol. 19:470–474. doi:10.1038/88150
911 • Murashige T, Skoog F. 1962. A revised medium for rapid growth and
912 bioassays with tobacco tissue cultures. Physiol Plant. 15:473–497.
913 doi:10.1111/j.1399-3054.1962.tb08052.x
914 • Nakata M, Ohme-Takagi M. 2014. Quantification of anthocyanin content.
915 Bio-Protoc. 4:1428–1440. doi:10.21769/BioProtoc.1098
916 • Noda Y, Kaneyuki T, Mori A, Packer L. 2002. Antioxidant activities of
917 pomegranate fruit extract and its anthocyanidins: delphinidin, cyanidin, and
918 pelargonidin. J Agric Food Chem. 50:166–171. doi:10.1021/jf0108765
919 • Park, J., Massa, A. N., Douches, D., Coombs, J., Akdemir, D., Yencho, G. C.,
920 Whitworth, J. L., & Novy, R. G. (2021). Linkage and QTL mapping for tuber
921 shape and specific gravity in a tetraploid mapping population of potato
922 representing the russet market class. BMC Plant Biology, 21(507).
923 https://doi.org/10.1186/s12870-021-03265-2
924 • Pradhan Mitra P, Loqué D. 2014. Histochemical staining of Arabidopsis
925 thaliana secondary cell wall elements. J Vis Exp. 87:51381.
926 doi:10.3791/51381
927 • Reinhart, B. J., Liu, T., Newell, N. R., Magnani, E., Huang, T., Kerstetter, R.,
928 Michaels, S., & Barton, M. K. (2013). Establishing a framework for the
929 Ad/Abaxial regulatory network of Arabidopsis: Asymmetric leaves2 and
930 REVOLUTA regulate auxin-related genes. The Plant Cell, 25(6), 2070–2085.
931 https://doi.org/10.1105/tpc.113.110387
932 • Roumeliotis E, Kloosterman B, Oortwijn M, Kohlen W, Bouwmeester HJ,
933 Visser RGF, Bachem CWB. 2012. The effects of auxin and strigolactones on
934 tuber initiation and stolon architecture in potato. J Exp Bot. 63:4539–4547.
935 doi:10.1093/jxb/ers132
936 • Sakuraba Y, Yanagisawa S. 2018. Light signalling-induced regulation of
937 nutrient acquisition and utilisation in plants. Semin Cell Dev Biol. 83:123–132.
938 doi:10.1016/j.semcdb.2017.12.014

939 • Sattelmacher B, Marschner H. 1978. Cytokinin activity in stolons and tubers
940 of Solanum tuberosum during the period of tuberization. Z Pflanzenernähr
941 Bodenkd. 44.
942 • Sessa G, Steindler C, Morelli G, Ruberti I. 1998. The Arabidopsis Athb-8, -9
943 and -14 genes are members of a small gene family coding for highly related
944 HD-ZIP proteins. Plant Mol Biol. 38.
945 • Seymour, G. B., Østergaard, L., Chapman, N. H., Knapp, S., & Martin, C.
946 (2013). Fruit development and ripening. Annual Review of Plant Biology, 64,
947 219–241. https://doi.org/10.1146/annurev-arplant-050312-120057
948 • Si, L., Chen, J., Huang, X., Gong, H., Luo, J., Hou, Q., Zhou, T., Lu, T., Zhu,
949 J., Shangguan, Y., Chen, E., Gong, C., Zhao, Q., Lu, Y., Weng, Q., Wang, Y.,
950 Han, B., & Wei, X. (2016). OsSPL13 controls grain size in cultivated rice.
951 Nature Genetics, 48(4), 447–456. https://doi.org/10.1038/ng.3518
952 • Singh A, Singh S, Panigrahi KCS, Reski R, Sarkar AK. 2014. Balanced
953 activity of microRNA166/165 and its target transcripts from the class III
954 homeodomain-leucine zipper family regulates root growth in Arabidopsis
955 thaliana. Plant Cell Rep. 33:945–953. doi:10.1007/s00299-014-1573-z
956 • Stembridge GE, Morrell G. 1972. Effect of gibberellins and 6-benzyladenine
957 on the shape and fruit set of 'Delicious' apples. J Am Soc Hort Sci. 97:464–
958 467.
959 • Tang D, Jia Y, Zhang J, Li H, Cheng L, Wang P, Bao Z, Liu Z, Feng S, Zhu X,
960 et al. 2022. Genome evolution and diversity of wild and cultivated potatoes.
961 Nature. 606:535–541.
962 • Todesco M, Rubio-Somoza I, Paz-Ares J, Weigel D. 2010. A collection of
963 target mimics for comprehensive analysis of microRNA function in
964 Arabidopsis thaliana. PLoS Genet. 6:e1001031.
965 doi:10.1371/journal.pgen.1001031
966 • Van der Knaap, E., & Østergaard, L. (2018). Shaping a fruit: Developmental
967 pathways that impact growth patterns. Seminars in Cell & Developmental
968 Biology, 79, 27–36. https://doi.org/10.1016/j.semcdb.2017.10.028
969 • Varkonyi-Gasic E, Wu R, Wood M, Walton EF, Hellens RP. 2007. Protocol: a
970 highly sensitive RT-PCR method for detection and quantification of
971 microRNAs. Plant Methods. 3:12. doi:10.1186/1746-4811-3-12

- Wang CK, Han PL, Zhao YW, Ji XL, Yu JQ, You CX, Hu DG, Hao YJ. 2020. Auxin regulates anthocyanin biosynthesis through the auxin repressor protein MdIAA26. Biochem Biophys Res Commun. 533:717–722. doi:10.1016/j.bbrc.2020.09.065
- Wang N, Xu HF, Jiang SH, Fang HC, Su MY, Zhang ZY, Zhang TL, Chen XS. 2018. Auxin regulates anthocyanin biosynthesis through the Aux/IAA–ARF signaling pathway in apple. Hortic Res. 5:59. doi:10.1038/s41438-018-0068-4
- Wang Y, Clevenger JP, Illa-Berenguer E, Meulia T, van der Knaap E, Sun L. 2019. A comparison of sun, ovate, fs8.1 and auxin application on tomato fruit shape and gene expression. Plant Cell Physiol. 60:1067–1081. doi:10.1093/pcp/pcz024
- Zhang J, Zhang H, Srivastava AK, Pan Y, Bai J, Fang J, Shi H, Zhu JK. 2018. Knockdown of rice microRNA166 confers drought resistance by causing leaf rolling and altering stem xylem development. Plant Physiol. 176:2082–2094. doi:10.1104/pp.17.01432
- Zhang, Z., Yang, T., Li, N., Tang, G., & Tang, J. (2024). MicroRNA166: Old players and new insights into crop agronomic traits improvement. Genes, 15(7), 944. https://doi.org/10.3390/genes15070944
- Zhao C, Ma J, Zhang Y, Yang S, Feng X, Yan J. 2022. The miR166-mediated regulatory module controls plant height by regulating gibberellic acid biosynthesis and catabolism in soybean. J Integr Plant Biol. 64:995–1006. doi:10.1111/jipb.13253
- Zierer, W., & Davies, P. J. (2021). Tuber and tuberous root development. Annual Review of Plant Biology, 72, 203–231.
- Zuker M. 2003. Mfold web server for nucleic acid folding and hybridization prediction. Nucleic Acids Res. 31:3406–3415.

Figure legends

Figure 1. Identification, Validation, and Expression Analysis of *miR166* in Potato

(A) RT-PCR of *miR166* precursors from shoot apex, leaves and stolons tissues of SD grown *Solanum tuberosum* ssp. *andigena*. (B-D) Quantification of precursor-a, -b, and -c levels from stolon-to-tuber transition stages (stolon, swollen stolon and mini-tuber)

1005 harvested from potato plants post 10 days of SD or LD induction. Relative transcript
1006 abundance of the gene expression in SD tissue is compared to LD stolons. Asterisks
1007 (one, two, three, and four) indicate significant differences at $p < 0.05$, $p < 0.01$,
1008 $p < 0.001$, and $p < 0.0001$, respectively, using Student's t-test. ns = not significant at
1009 $p > 0.05$. *StEIF3e* was used as a reference gene. Detection (E) and relative fold change
1010 (F) of mature *miR166* from leaves and stolon tissues of SD grown (7 days post
1011 induction, 7 dpi) *Solanum tuberosum* ssp. *andigena* by stem-loop RT-PCR. (G)
1012 Relative abundance of *miR166* in stolon-to-tuber transition stages. *StU6* was used for
1013 normalization. Error bars indicate (±) SEM of three biological replicates, each with
1014 three technical replicates. Asterisks (one, two, three, and four) indicate significant
1015 differences at $p < 0.05$, $p < 0.01$, $p < 0.001$, and $p < 0.0001$, respectively, using
1016 Student's t-test. ns = not significant at $p > 0.05$. (H) Confirmation of HD-ZIP III
1017 targets of *miR166*. Partial mRNA sequence of *ICU1*, *ICU2*, *REV*, *PHB*, *PHV*, and
1018 *HB8* aligned with *miR166*, numbers denote the fraction of cloned cleavage products
1019 that terminate at different positions (arrows).
1020
1021 **Figure 2. Knockdown of microRNA166 causes pleiotropic phenotypic changes** (A)
1022 Expression levels of *miR166* in mimicry lines (KD #2, KD #3) compared to WT. *StU6*
1023 was used as a reference gene. Error bars indicate standard error of means (SEM) from
1024 three biological replicates (n=3). Asterisks (one, two, three, and four) indicate
1025 significant differences at $p < 0.05$, $p < 0.01$, $p < 0.001$, and $p < 0.0001$, respectively,
1026 using Student's t-test. ns = not significant at $p > 0.05$. (B) Plant architecture of *miR166*
1027 KD lines along with WT. Scale bar= 5 cm. Plant height (C), number of nodes (D) and
1028 internodal distance (E) of *miR166* KD lines in comparison with WT (n=10). (F)
1029 Photographs of 8-week old LD grown plants, showing reduced leaf curvature in KD
1030 plants (arrows). Scale bar= 2 cm. (G) The longitudinal and transverse curvature
1031 indices of leaves emerging from the 5th-node of 8-week old plants (n=10). Asterisks
1032 (one, two, three and four) indicate significant differences at $p < 0.05$, $p<0.01$, $p<0.001$
1033 and $p<0.0001$, respectively, using one-way ANOVA. ns= not significant at <0.05. (H)
1034 Transverse sections of stem from *miR166* KD and WT LD grown plants. Scale bar=
1035 50 microns.
1036
1037 **Figure 3. *miR166* knockdown lines have elongated, pigmented tubers with**
1038 **reduced tuber productivity** (A) Tuber weight per plant and (B) average tuber

1039 number of *miR166* KD lines compared to WT. Data was taken from soil grown plants
1040 after two months of SD induction, and plotted from 14 individual plants per line. (C)
1041 Representative tuber images from *miR166* KD lines compared to WT, *miR166* KD
1042 tubers are elongated, and accumulate anthocyanin pigments in their peels. Cut tubers
1043 scale bar= 1 cm; Intact tubers scale bar= 3cm. The sphericity index (D) and average
1044 tuber volume (E) of *miR166* KD tubers in comparison to WT. The data is plotted for
1045 30 tubers from each line. Asterisks (one, two, three and four) indicate significant
1046 differences at $p < 0.05$, $p<0.01$, $p<0.001$ and $p<0.0001$, respectively, using one-way
1047 ANOVA. ns= not significant at <0.05. (F) Quantification of cyanidin 3-glucoside,
1048 pelargonidin 3-glucoside and delphinidin 3-glucoside from the tuber peels of WT and
1049 *miR166* KD. The mean value (n = 4) ± SEM is presented. Asterisks (one, two, three,
1050 and four) indicate significant differences at $p < 0.05$, $p < 0.01$, $p < 0.001$, and
1051 $p < 0.0001$, respectively, using one-way ANOVA. ns = not significant at $p > 0.05$. (G)
1052 Relative fold change of key tuber marker genes in the stolons (7 days SD) of *miR166*
1053 KD, compared to the WT. Error bars indicate standard error of means (SEM) from
1054 three biological replicates (n=3). Asterisks (one, two, three, and four) indicate
1055 significant differences at $p < 0.05$, $p < 0.01$, $p < 0.001$, and $p < 0.0001$, respectively,
1056 using Student's t-test. ns = not significant at $p > 0.05$. (H) *In vitro* tuber induction
1057 assay for *miR166* KD lines along with WT.
1058
1059 **Figure 4. RNA-Seq analysis reveals differentially expressed genes in swollen and**
1060 **sub-swollen part of tuberizing stolons** (A) Stolon-to-tuber transition stages as seen
1061 in the WT and *miR166* KD #3. (B) A schematic illustration to depict the tissue
1062 collection carried out for RNA-sequencing analysis. The Head and sub-swelling (SSR)
1063 region were collected individually from WT and KD #3 stolons from plants grown
1064 under SD photoperiod for 12 days. (C) Venn diagram shows the summary of unique
1065 and shared genes expressed in KD #3 and WT tissues (Head *vs*. SSR). (D-E) The heat
1066 map represents differential expression of genes involved in Auxin, GA and CK
1067 metabolism and transport. Numbers inside the box represent variance stabilized
1068 transformed (*vs*T) values. Relative quantification of IAA- 3 (F) and GA_3 (G) from the
1069 Stolon, Head and SSR tissues from WT and *miR166* KD #3.
1070
1071 **Figure 5. REVOLUTA affects tuberization** (A) Primary PCR product from
1072 modified 5′ RLM-RACE, to confirm *REV* as a target of *miR166* in potato. (B)

1073 Relative fold change of *REV* in differentiating stolons from WT plants. (C) Relative
1074 fold change of *REV* in stolons from *miR166* KD and OE lines. *StEIF3e* was used as
1075 reference gene. Error bars indicate standard error of means (SEM) from three
1076 biological replicates (n=3). Asterisks (one, two, three, and four) indicate significant
1077 differences at $p < 0.05$, $p < 0.01$, $p < 0.001$, and $p < 0.0001$, respectively, using
1078 Student's t-test. ns = not significant at $p > 0.05$. (D) Promoter expression of *StREV* in
1079 *promStREV:uidA* transgenic lines. (i) *in vitro* plant, (ii) axillary node, (iii) shoot-
1080 forming stolon, (iv) swollen stolon, (v) T.S. of swollen stolon, and (vi) mini-tuber.
1081 Scale bar= 1000 um for (i) and (vi); Scale bar= 500um for (ii)- (v). (E) Longitudinal
1082 sections of shoot apex from WT plants, black arrow heads show polarized localization
1083 of REV transcripts in developing leaves. Scale bar= 100 um. Tuber productivity and
1084 tuber numbers (F-H) from REV AS lines, relative to the WT. Scale bar= 2 cm.
1085 Asterisks (one, two, three and four) indicate significant differences at $p < 0.05$, $p<0.01$,
1086 $p<0.001$ and $p<0.0001$, respectively, using one-way ANOVA. ns= not significant at
1087 <0.05.
1088
1089 **Figure 6.** (A) Promoters of auxin biosynthesis genes harbor the AT(C/G)AT sequence,
1090 a core motif of HD-ZIP III binding site. (B) RT-qPCR of *REV*-AS stolons show
1091 reduced transcript abundance of auxin biosynthesis genes. Dual luciferase assay (C)
1092 shows approximately 10 fold upregulation of promoter *StYUC7* in presence of
1093 StREVOLUTA. A *5'm-StREV-FLAG* construct was used that is resistant to cleavage
1094 by *miR166*. Asterisks (one, two, three and four) indicate significant differences at
1095 $p < 0.05$, $p<0.01$, $p<0.001$ and $p<0.0001$, respectively, using one-way ANOVA. ns=
1096 not significant at <0.05. (D) Yeast-mated clones containing *StREV* prey protein and
1097 prStYUC7 bait, or StARF10 prey protein and *prStGH3.6* bait (positive control) grew
1098 in media containing up to 80 mM 3-amino-1,2,4-triazole (3-AT), indicating the
1099 binding of StREV to *StYUC7* promoter. The p53 binding site was used as a negative
1100 control. The yeast-mated clones harboring StREV and *p53* did not grow on the
1101 selection media, suggesting that there is no interaction between the *p53* binding site
1102 and StREV protein.
1103
1104 **Figure 7.** A proposed model for the role(s) of *miR166*-REVOLUTA-auxin module in
1105 potato tuberization. *miR166* in potato targets the *StREVOLUTA*. StREV activates the
1106 expression of auxin biosynthesis gene- *StYUCCA7*. In MIM166 line, decreased levels

1107 of *miR166* leads to increased/ectopic *REV* expression, causing perturbed auxin
1108 biosynthesis and transport leading to the development of elongated tubers. In *StREV*-
1109 antisense, the tubers are spherical, with reduced size and productivity.

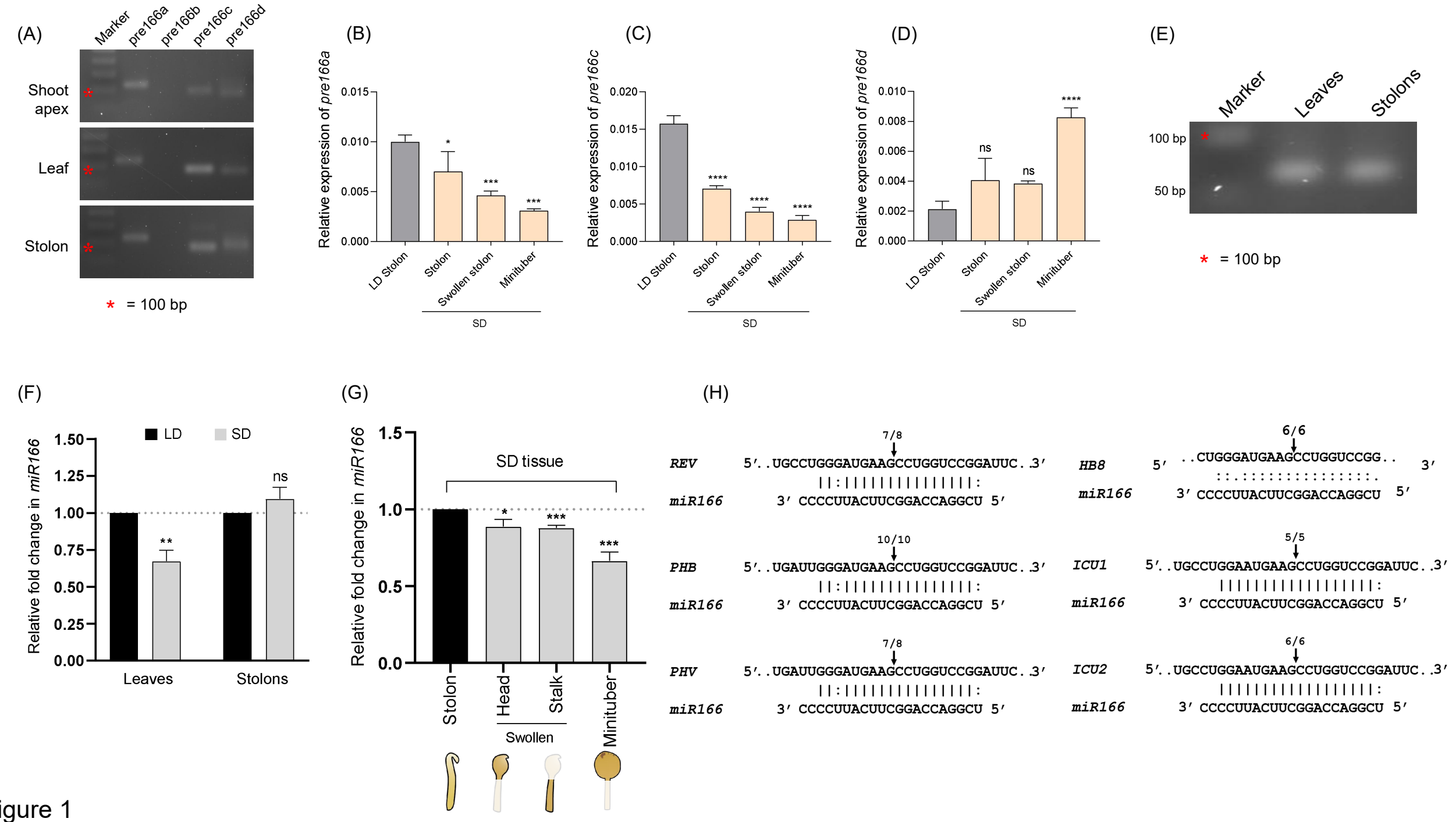
(A)
Marker
pre166a
pre166b
pre166c
pre166d
Shoot apex
Leaf
Stolon
* = 100 bp
(B)
Relative expression of pre166a
0.015
0.010
0.005
0.000
*
***
***
LD Stolon
Stolon
Swollen stolon
Minituber
SD
(C)
Relative expression of pre166c
0.020
0.015
0.010
0.005
0.000
****
****
****
LD Stolon
Stolon
Swollen stolon
Minituber
SD
(D)
Relative expression of pre166d
0.010
0.008
0.006
0.004
0.002
0.000
ns
ns
****
LD Stolon
Stolon
Swollen stolon
Minituber
SD
(E)
Marker
Leaves
Stolons
100 bp
50 bp
* = 100 bp
(F)
LD
SD
Relative fold change in miR166
1.50
1.25
1.00
0.75
0.50
0.25
0.00
**
ns
Leaves
Stolons
(G)
Relative fold change in miR166
1.5
1.0
0.5
0.0
SD tissue
*
***
***
Stolon
Head
Stalk
Minituber
Swollen
(H)
REV 5′..UGCCUGGGAUGAAGCCUGGUCCGGAUUC..3′
7/8
miR166 3′ CCCCUUACUUCGGACCAGGCU 5′
PHB 5′..UGAUUGGGAUGAAGCCUGGUCCGGAUUC..3′
10/10
miR166 3′ CCCCUUACUUCGGACCAGGCU 5′
PHV 5′..UGAUUGGGAUGAAGCCUGGUCCGGAUUC..3′
7/8
miR166 3′ CCCCUUACUUCGGACCAGGCU 5′
HB8 5′ ..CUGGGAUGAAGCCUGGUCCGG.. 3′
6/6
miR166 3′ CCCCUUACUUCGGACCAGGCU 5′
ICU1 5′..UGCCUGGAAUGAAGCCUGGUCCGGAUUC..3′
5/5
miR166 3′ CCCCUUACUUCGGACCAGGCU 5′
ICU2 5′..UGCCUGGAAUGAAGCCUGGUCCGGAUUC..3′
6/6
miR166 3′ CCCCUUACUUCGGACCAGGCU 5′

Figure 1

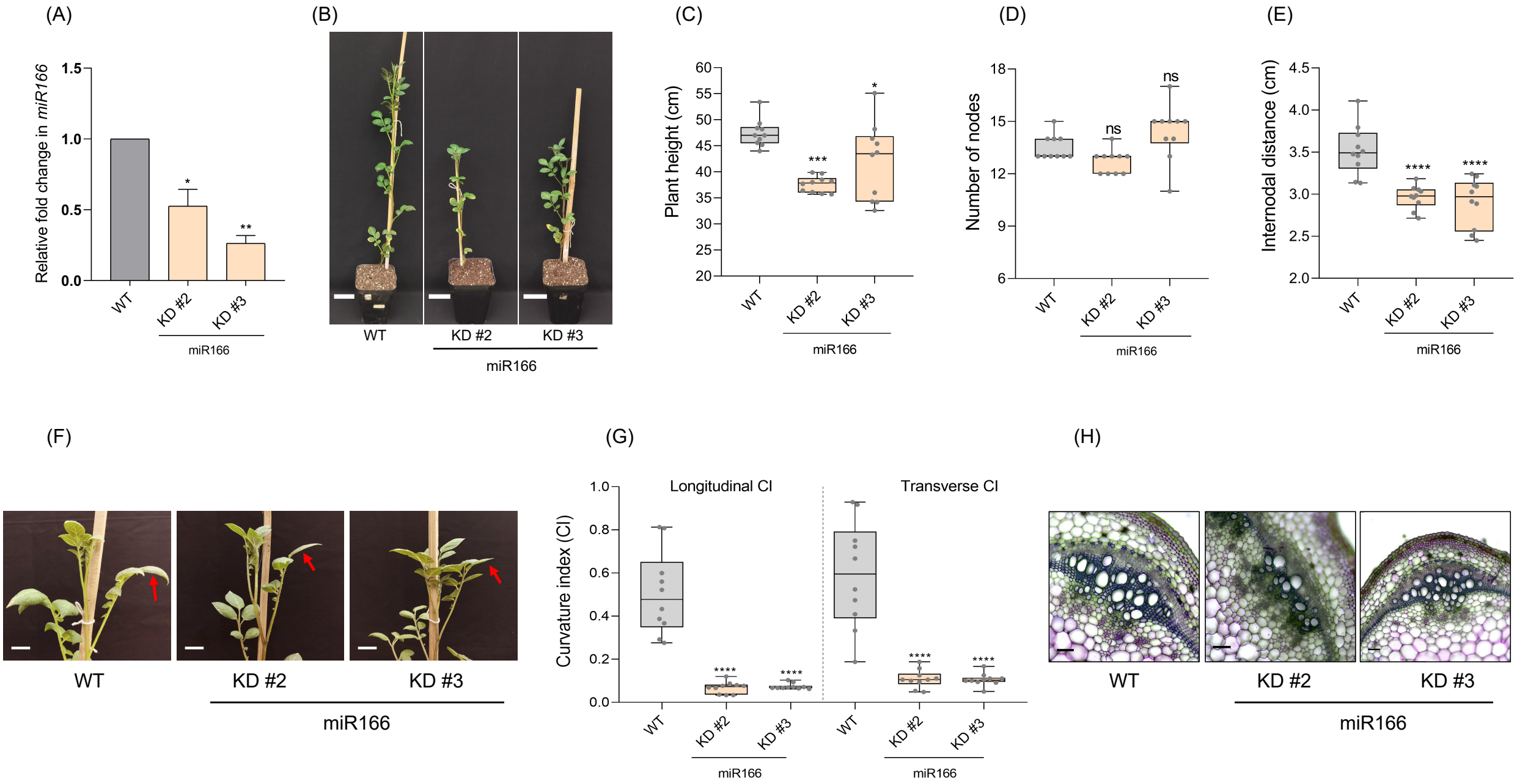
(A)
Relative fold change in miR166
1.5
1.0
0.5
0.0
*
**
WT
KD #2
KD #3
miR166
(B)
WT
KD #2
KD #3
miR166
(C)
Plant height (cm)
60
55
50
45
40
35
30
25
20
***
*
WT
KD #2
KD #3
miR166
(D)
Number of nodes
18
15
12
9
6
ns
ns
WT
KD #2
KD #3
miR166
(E)
Internodal distance (cm)
4.5
4.0
3.5
3.0
2.5
2.0
****
****
WT
KD #2
KD #3
miR166
(F)
WT
KD #2
KD #3
miR166
(G)
Curvature index (CI)
1.0
0.8
0.6
0.4
0.2
0.0
Longitudinal CI
Transverse CI
****
****
****
****
WT
KD #2
KD #3
WT
KD #2
KD #3
miR166
miR166
(H)
WT
KD #2
KD #3
miR166

Figure 2

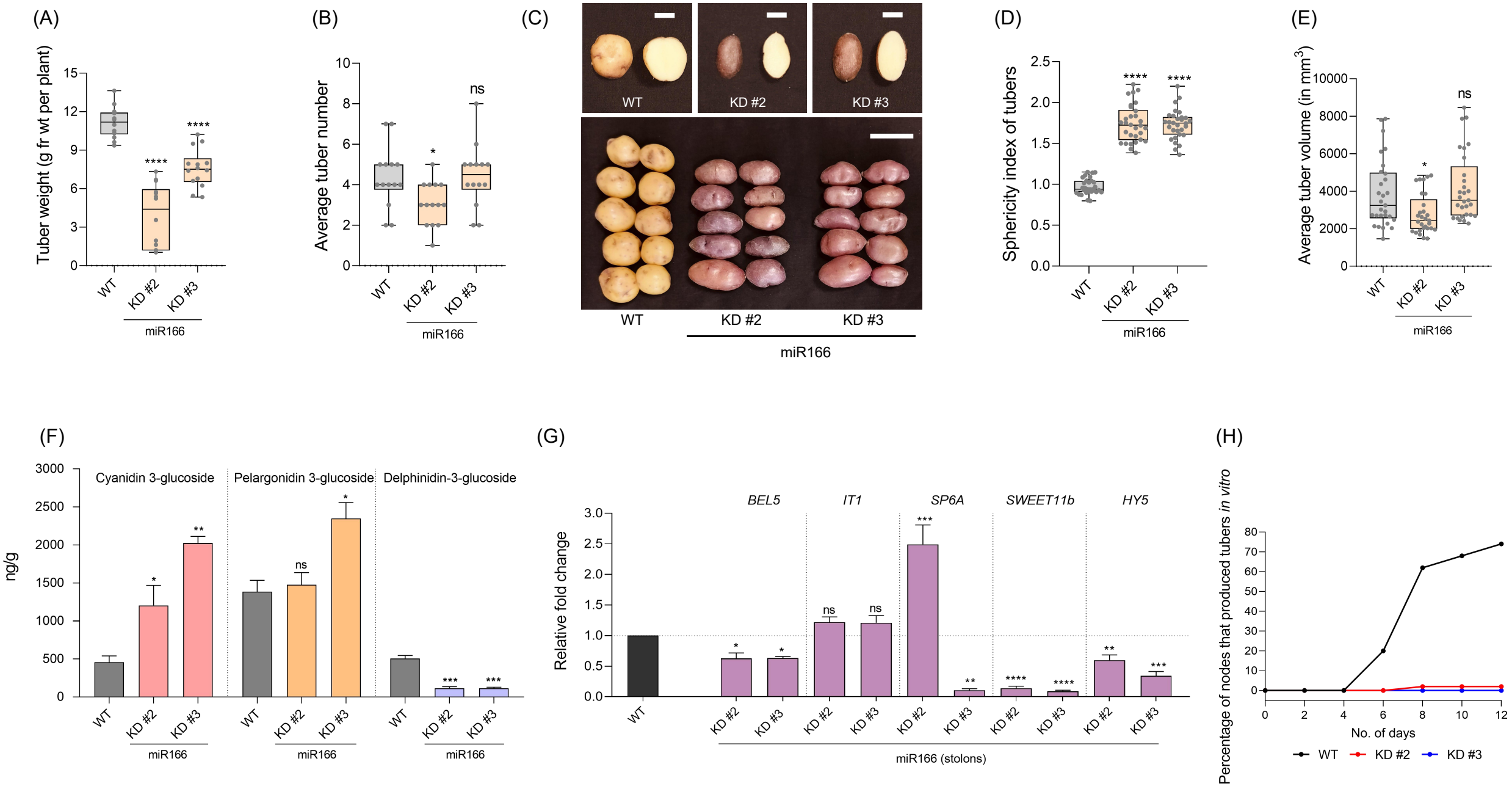
(A)
Tuber weight (g fr wt per plant)
WT
KD #2
KD #3
miR166
(B)
Average tuber number
ns
(C)
WT
KD #2
KD #3
miR166
(D)
Sphericity index of tubers
(E)
Average tuber volume (in mm3)
(F)
ng/g
Cyanidin 3-glucoside
Pelargonidin 3-glucoside
Delphinidin-3-glucoside
(G)
Relative fold change
BEL5
IT1
SP6A
SWEET11b
HY5
miR166 (stolons)
(H)
Percentage of nodes that produced tubers in vitro
No. of days

Figure 3

(A)

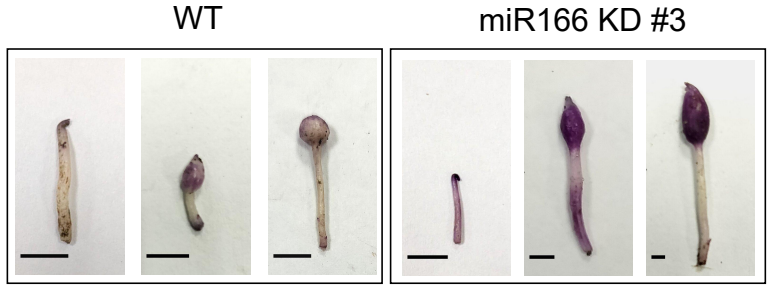

(B)

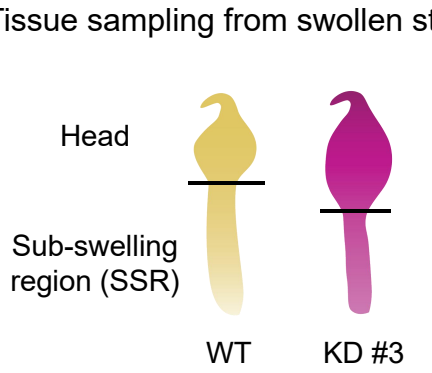

(C)

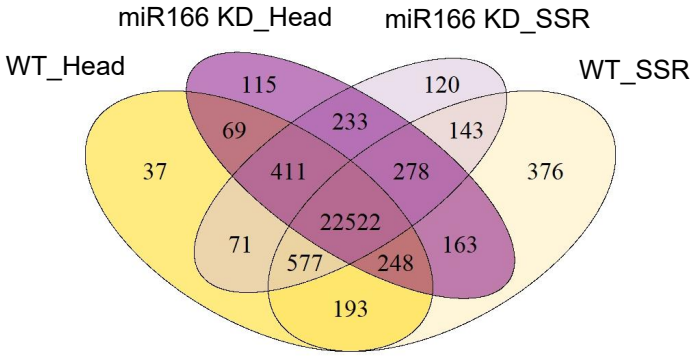

(D)

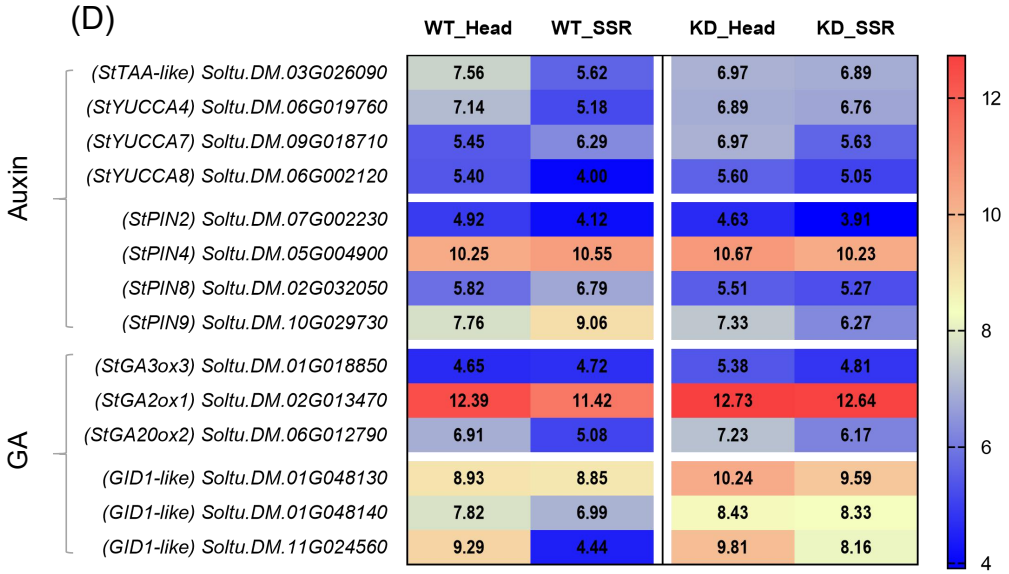

(E)

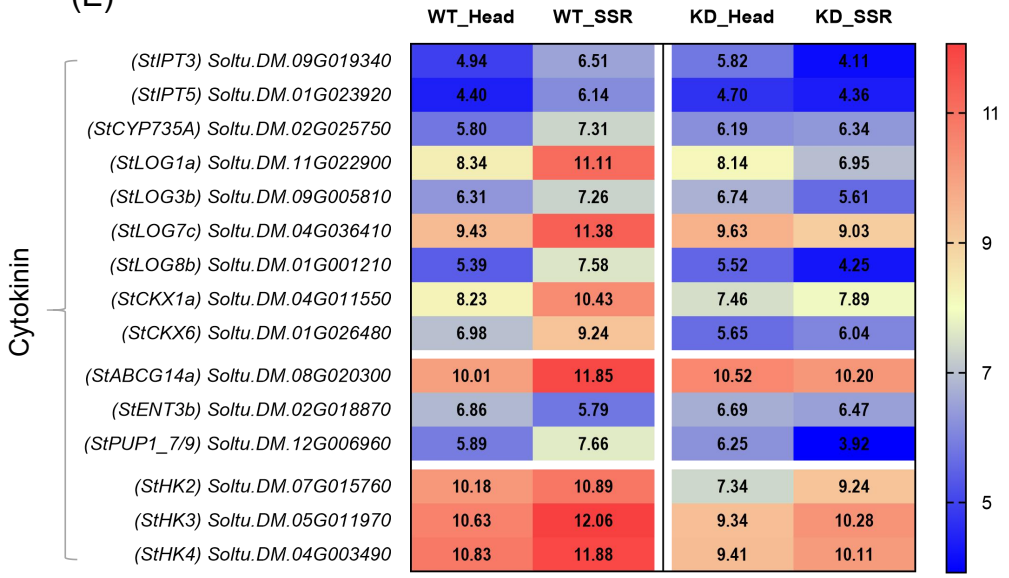

(F)

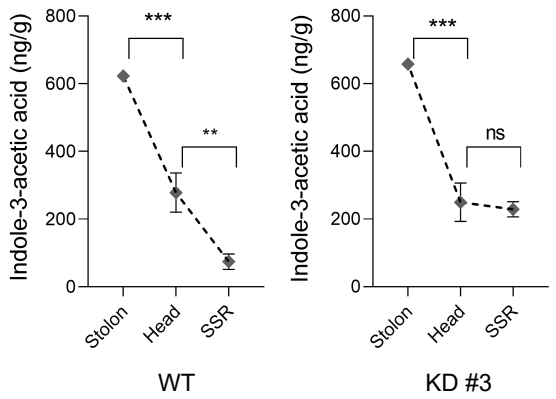

(G)

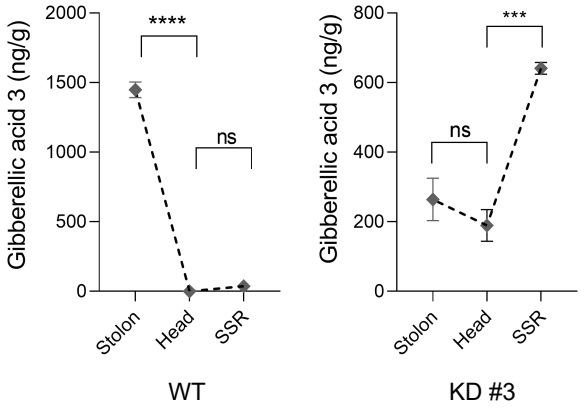

Figure 4

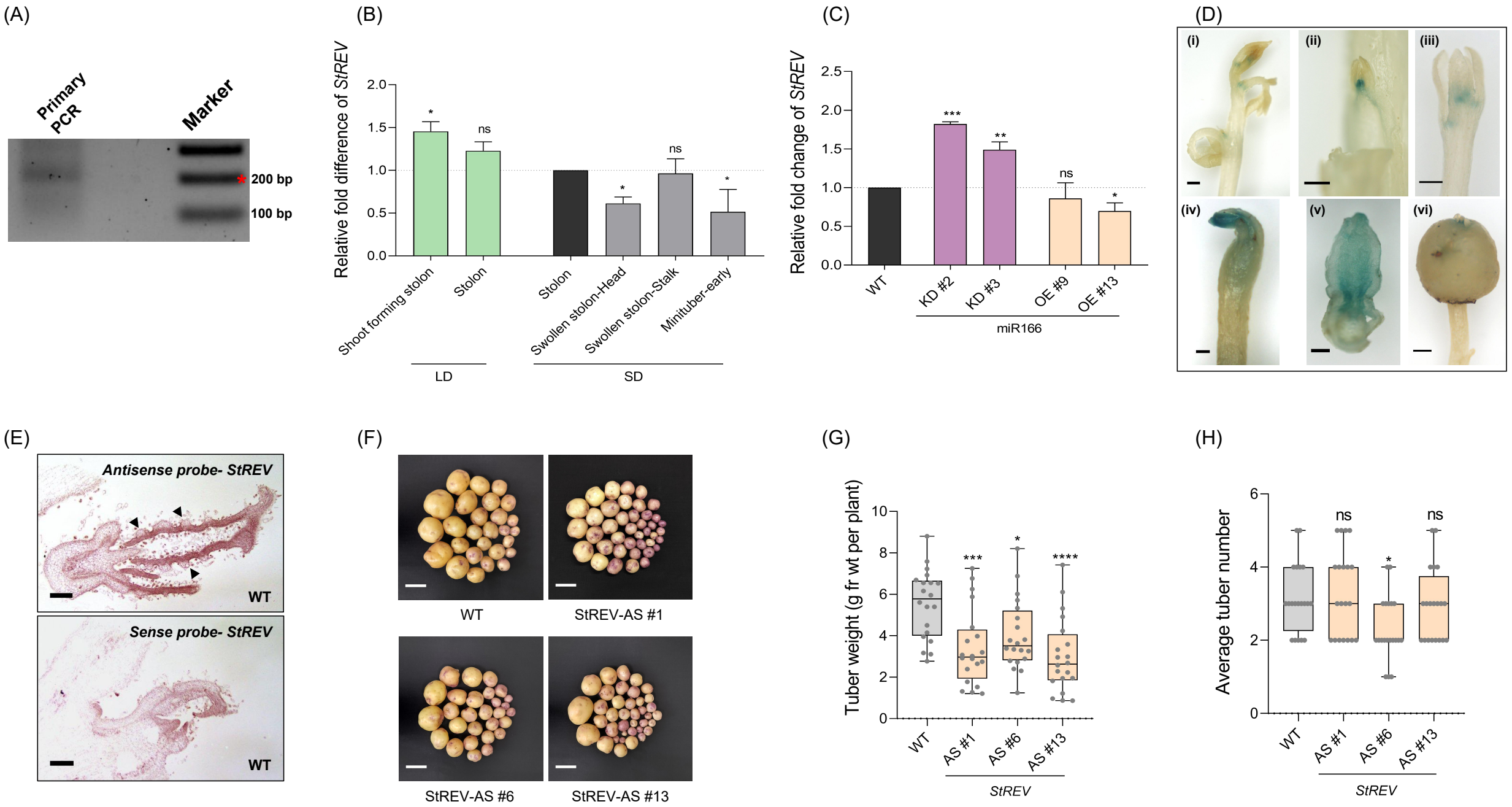
(A)
Primary PCR
Marker
200 bp
100 bp
(B)
Relative fold difference of StREV
2.0
1.5
1.0
0.5
0.0
*
ns
*
ns
*
Shoot forming stolon
Stolon
Stolon
Swollen stolon-Head
Swollen stolon-Stalk
Minituber-early
LD
SD
(C)
Relative fold change of StREV
2.5
2.0
1.5
1.0
0.5
0.0
***
**
ns
*
WT
KD #2
KD #3
OE #9
OE #13
miR166
(D)
(i)
(ii)
(iii)
(iv)
(v)
(vi)
(E)
Antisense probe- StREV
WT
Sense probe- StREV
WT
(F)
WT
StREV-AS #1
StREV-AS #6
StREV-AS #13
(G)
Tuber weight (g fr wt per plant)
10
8
6
4
2
0
***
*
****
WT
AS #1
AS #6
AS #13
StREV
(H)
Average tuber number
6
4
2
0
ns
*
ns
WT
AS #1
AS #6
AS #13
StREV

Figure 5

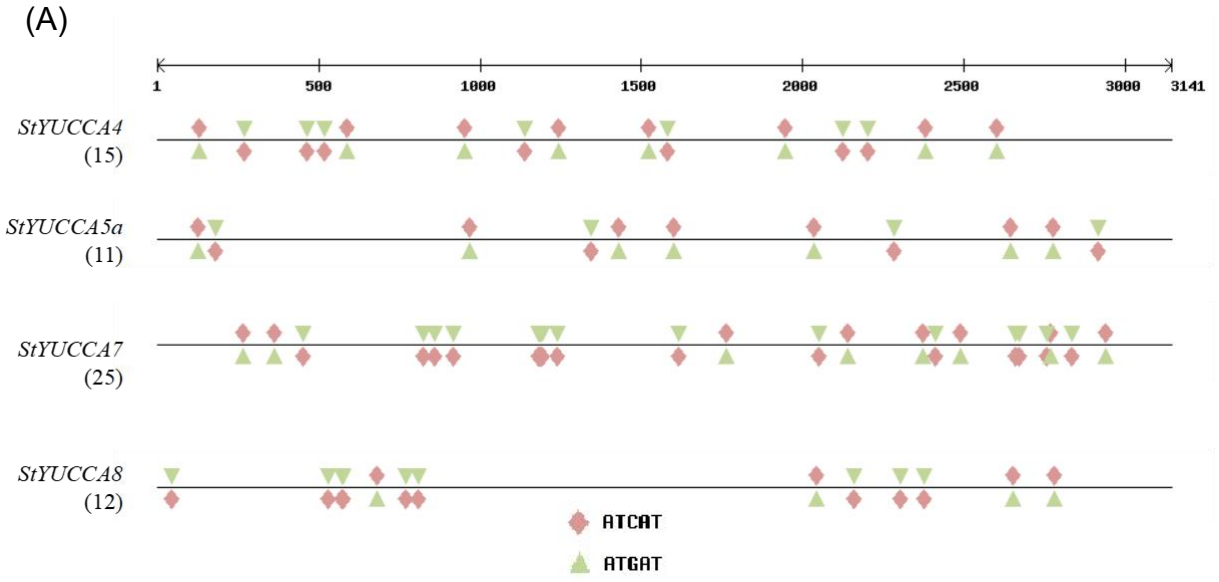
(A)
1
500
1000
1500
2000
2500
3000
3141
StYUCCA4
(15)
StYUCCA5a
(11)
StYUCCA7
(25)
StYUCCA8
(12)
ATCAT
ATGAT

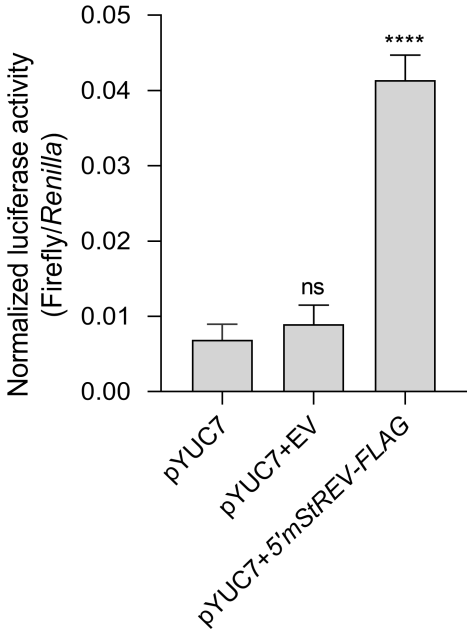
(C)
Normalized luciferase activity
(Firefly/Renilla)
0.05
0.04
0.03
0.02
0.01
0.00
****
ns
pYUC7
pYUC7+EV
pYUC7+5'mStREV-FLAG

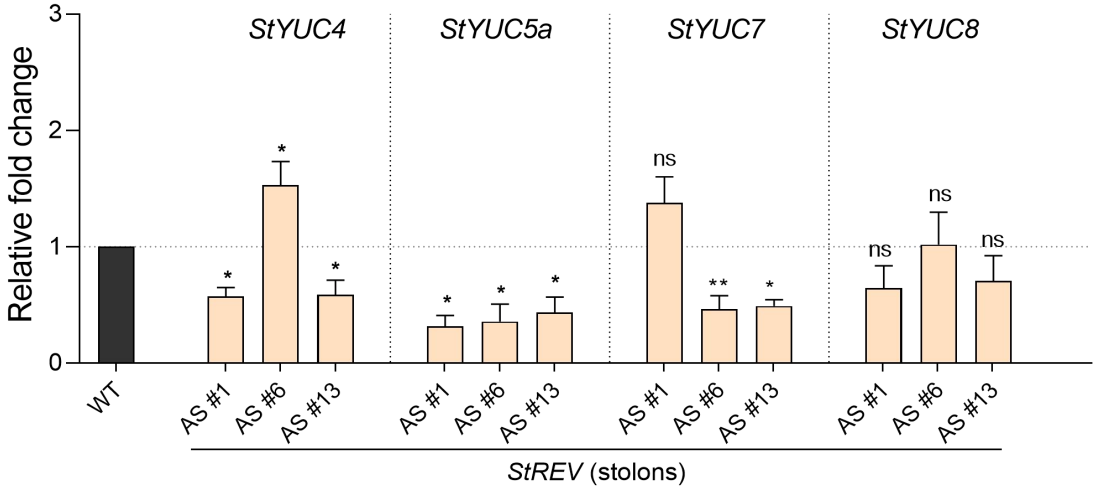
(B)
Relative fold change
3
2
1
0
StYUC4
StYUC5a
StYUC7
StYUC8
WT
AS #1
AS #6
AS #13
StREV (stolons)

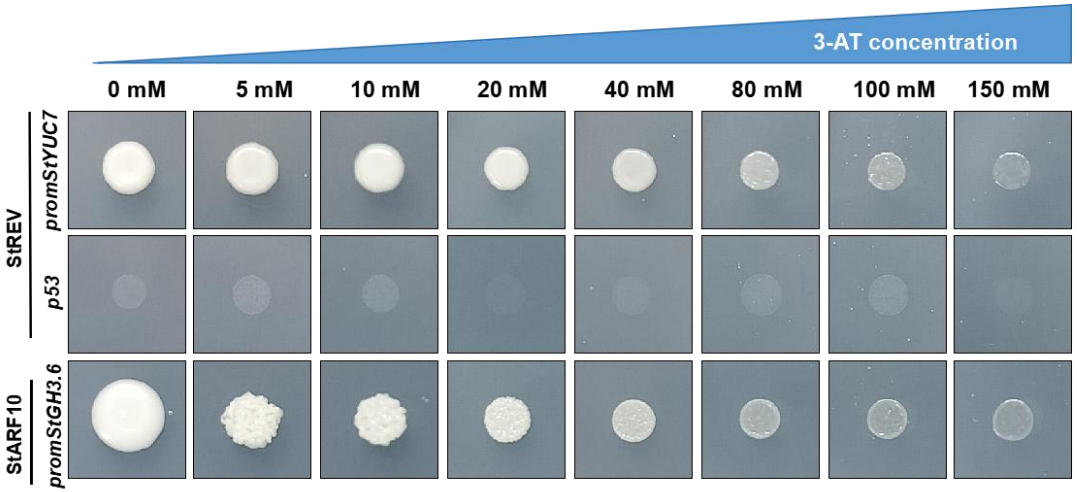
(D)
3-AT concentration
0 mM
5 mM
10 mM
20 mM
40 mM
80 mM
100 mM
150 mM
StREV
promStYUC7
p53
StARF10
promStGH3.6

Figure 6

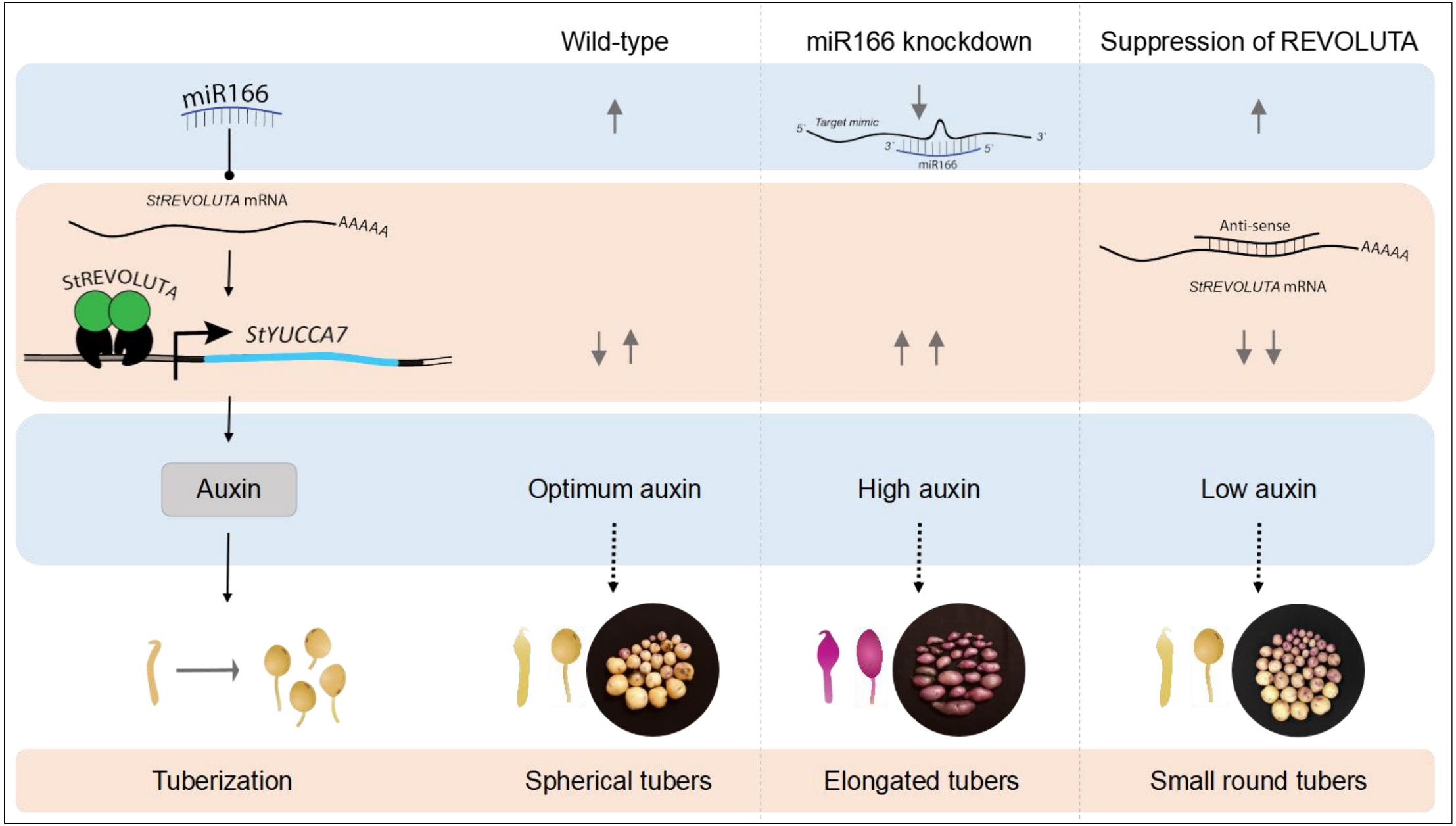
Wild-type
miR166 knockdown
Suppression of REVOLUTA
miR166
Target mimic
5`
3`
3`
5`
miR166
StREVOLUTA mRNA
AAAAA
Anti-sense
AAAAA
StREVOLUTA mRNA
StREVOLUTA
StYUCCA7
Auxin
Optimum auxin
High auxin
Low auxin
Tuberization
Spherical tubers
Elongated tubers
Small round tubers

Figure 7